THE GEOLOGICAL SOCIETY OF AMERICA®

Sedimentation, earthquakes, and tsunamis in a shallow, muddy epeiric sea: Grinnell Formation (Belt Supergroup, ca. 1.45 Ga), western North America

Brian R. Pratt[1,†] and Juan J. Ponce[2,†]
[1]*Department of Geological Sciences, University of Saskatchewan, Saskatoon, Saskatchewan S7N 5E2, Canada*
[2]*Instituto de Investigación en Paleobiología y Geología, Universidad Nacional de Río Negro, Isidro Lobo y Belgrano, 8332 Roca, Río Negro, Argentina*

ABSTRACT

Interpreting the deposits of ancient epeiric seas presents unique challenges because of the lack of direct modern analogs. Whereas many such seas were tectonically relatively quiescent, and successions are comparatively thin and punctuated by numerous sedimentary breaks, the Mesoproterozoic Belt Basin of western North America was structurally active and experienced dramatic and continuous subsidence and sediment accumulation. The Grinnell Formation (ca. 1.45 Ga) in the lower part of the Belt Supergroup affords an opportunity to explore the interplay between sedimentation and syndepositional tectonics in a low-energy, lake-like setting. The formation is a thick, vivid, red- to maroon-colored mudstone-dominated unit that crops out in northwestern Montana and adjacent southwestern Alberta, Canada. The mudstone, or argillite, consists of laminated siltstone and claystone, with normal grading, local low-amplitude, short-wavelength symmetrical ripples, and intercalations of thin tabular intraclasts. These intraclasts suggest that the muds acquired a degree of stiffness on the seafloor. Halite crystal molds and casts are present sporadically on bedding surfaces. Beds are pervasively cut by mudcracks exhibiting a wide variety of patterns in plan view, ranging from polygonal to linear to spindle-shaped. These vertical to subvertical cracks are filled with upward-injected mud and small claystone intraclasts. Variably interbedded are individual, bundled, or amalgamated, thin to medium beds of white, cross-laminated, medium- to coarse-grained sandstone, or quartzite. These are composed of rounded quartz grains, typically with subangular to rounded mudstone intraclasts. Either or both the bottoms and tops of sandstone beds commonly show sandstone dikes indicative of downward and upward injection. Both the mudcracks and the sandstone dikes are seismites, the result of mud shrinkage and sediment injection during earthquakes. An origin via passive desiccation or syneresis is not supported, and there is no evidence that the sediments were deposited on alluvial plains, tidal flats, or playas, as has been universally assumed. Rather, deposition occurred in relatively low-energy conditions at the limit of ambient storm wave base. The halite is not from in situ evaporation but precipitated from hypersaline brines that were concentrated in nearshore areas and flowed into the basin causing temporary density stratification. Sandstone beds are not fluvial. Instead, they consist of allochthonous sediment and record a combination of unidirectional and oscillatory currents. The rounded nature of the sand and irregular stratigraphic distribution of the sandstone intervals are explained not by deltaic influx or as tempestites but as coastal sands delivered from the eastern side of the basin by off-surge from episodic tsunamis generated by normal faulting mainly in the basin center. The sands were commonly reworked by subsequent tsunami onrush, off-surge, seiching, and weak storm-induced wave action. Although the Grinnell Formation might appear superficially to have the typical hallmarks of a subaerial mudflat deposit, its attributes in detail reveal that sedimentation and deformation took place in an entirely submerged setting. This is relevant for the deposits of other ancient epeiric seas as well as continental shelves, and it should invite reconsideration of comparable successions.

INTRODUCTION

Understanding of the sedimentologic, oceanographic, and climatologic dynamics of large, shallow epeiric seas in low-relief continental interiors, be they sag basins, rift basins, or foreland basins, can be challenging in part because no direct modern analogs exist (e.g., Shaw, 1964; Irwin, 1965; Pratt and Holmden, 2008; Pratt and Haidl, 2008; Schieber, 2016). Consequently, coastal and shallow-marine processes understood from present-day continental shelves may not be wholly applicable, especially for seas that were not fully connected to the open ocean and if circulation was sluggish. In addition, different paleoclimatic regimes would have governed meteorological phenomena such as frequency and strength of storms. The Mesoproterozoic Belt Basin of western North America is no exception, and it has the added characteristic of predating the advent of animals by almost a billion years and therefore existing during a time of a simplified carbon cycle, under different atmospheric conditions, and with waters of a composition perhaps not exactly the same as that of present-day seawater.

The Grinnell Formation in the lower part of the Belt Supergroup, exposed in the Rocky Mountains of northwestern Montana and adjacent southwestern Alberta, is striking in its resplendent red to maroon color (Fig. 1). These rocks have been much admired by generations of geologists, especially for their ubiquitous mudcracks, which have been universally taken as the product of subaerial exposure and desiccation.

The purpose of this paper is to present a detailed description of the Grinnell Formation and propose a novel interpretation of the processes of sediment deposition and deformation. This environmental interpretation combines

†brian.pratt@usask.ca; jponce@unrn.edu.ar.

GSA Bulletin; https://doi.org/10.1130/B35012.1; 25 figures.

Figure 1. Panoramic view eastward from the summit of Swiftcurrent Mountain (2571 m), Glacier National Park, northwestern Montana. The Grinnell Formation is the maroon-colored unit in the middle distance on the flank of Altyn Peak north of Swiftcurrent Lake. Below it is the greenish gray-colored Appekunny Formation. Above it is the thin, gray-colored Empire Formation, succeeded by the thick, tan-colored Helena Formation, which forms the slope and cliff of the northern flank of Mount Grinnell to the right; the exposure of Grinnell Formation beyond is on Allen Mountain. Lake Sherburne lies in the distance.

the effects of turbidity currents, hypopycnal plumes, storms, earthquakes, and tsunamis in a consistently submerged albeit shallow, lake-like sea. This study suggests that other stratigraphic units may exhibit comparable features, especially evidence for syndepositional tectonic activity in the form of seismites and tsunamites, that may have been heretofore underappreciated or gone unrecognized.

GEOLOGICAL SETTING

Belt Basin

The Mesoproterozoic Belt Supergroup (Purcell Supergroup in Canada) is exposed in a region straddling southwestern Alberta, southeastern British Columbia, western Montana, and northern Idaho (Fig. 2A). The Belt Basin was at least some 200,000 km^2 in area, extending eastward in its early phase and forming the Helena embayment in central Montana. As subsidence continued, the basin likely expanded considerably farther than is suggested by present-day outcrop distribution (Pratt, 2001). It was semi-enclosed and has been interpreted as a lake (Winston, 1986b, 1990, 2007), but it probably opened to the ocean to the northwest (e.g., Ross et al., 1992; Winston and Link, 1993; Chandler, 2000; Pratt, 2001). The basin existed for a relatively short span of geological time, from ca. 1.48 Ga to ca. 1.25 Ga (Lydon, 2000, 2007; Chandler, 2000; Sears, 2007b; Pratt, 2017). It was characterized by rapid and seemingly continuous subsidence for some 25 m.y., which slowly tapered off, resulting in nearly 20 km of strata in the central area, thinning to some 5–8 km in the northeast (e.g., Winston and Link, 1993; Lydon, 2000, 2007). The calculated sedimentation rate suggests that the varve-like layering may well be annual (Pratt, 2001, 2017). Several major normal faults oriented roughly west-east resulted in development of a central horst, a northern half graben, and a southern graben (Sears, 2007b), as well as the Helena embayment (Winston, 1986b, 1986c). Large changes in thickness of stratigraphic units over short distances indicate that syndepositional normal faulting took place along these west-east faults and subsidiary northwest-southeast–trending lineaments in the central part of the basin, as well as generating frequent synsedimentary seismicity (Pratt, 1998b, 2001). The northern side of the basin also experienced syndepositional faulting with significant displacement (Turner et al., 2000; Gardner, 2008). However, the high sedimentation rate probably maintained an overall low-relief topography for the basin floor.

The initially rapid subsidence and the Moyie sills in the lower part of the Belt Supergroup on the northern side of the basin suggest that the Belt Basin was formed by intracratonic rifting (e.g., Höy, 1989). This may have been caused by oblique collision of the more or less coherent Mawson (East Antarctic) and Australian cratons with present-day western and northwestern Laurentia to form the putative Mesoproterozoic supercontinent Columbia (= Nuna) as it moved paleo-northward (Pisarevsky et al., 2014; Pehrsson et al., 2016).

Due to this collision, substantial uplift to the west is considered to have been the source for most of the fine-grained sediment in the lower and middle portions of the Belt Supergroup yielding detrital zircon ages of ca. 1610–1500 Ma (Ross and Villeneuve, 2003; Link et al., 2007). As the western source began to decline, zircon populations in the ca. 1790–1655 Ma range, which predominate in the Missoula Group, were derived from basement terranes to the south (Link et al., 2007, 2016). Archean zircons in coarser sandstones in the Altyn, Appekunny, Grinnell, Helena, and Wallace Formations on the eastern side of the basin were derived from the adjacent basement (Ross and Villeneuve, 2003). A minor population ca. 1450 Ma in age in the Piegan Group corresponds to syndepositional magmatism, which is also recorded by the presence of a tuff bed at Logan Pass and in the Purcell Lava (Link et al., 2007).

Stratigraphy

The Belt Supergroup is subdivided into four groups: the Lower Belt, the Ravalli Group, the Piegan Group (or "middle Belt carbonate" of some past usage), and the Missoula Group (Fig. 3; e.g., Winston and Link, 1993; Winston, 2007). The Grinnell and Empire Formations comprise the Ravalli Group in the northeastern side of the basin, although some schemes place the Appekunny Formation in the lower Ravalli Group (Harrison et al., 1993; Winston and Sears, 2013). This is equivalent to the Creston Formation to the west in southeastern British Columbia (Hein and McMechan, 1994), and the Spokane Formation in west-central Montana south of Glacier National Park (Winston and Link, 1993). The Grinnell Formation is correlated with the Burke, Revett, and St. Regis Formations in western Montana and northern Idaho (Winston, 1986a, 1989a, 1989b, 2016; Winston and Link, 1993). The succession is overwhelmingly dominated by fine-grained siliciclastic facies, but carbonates forming part of the Lower Belt were deposited on the northeastern side and

in central Montana, and the younger Helena and Wallace Formations make up the basin-wide Piegan Group. Whereas the clay and silt were mainly sourced from the west, coarser sand came from the east (Winston and Link, 1993; Pratt, 2001; Ross and Villeneuve, 2003; Winston, 2007). The rocks are well preserved on the eastern side, having undergone no more than sub-biotite-grade greenschist-facies metamorphism via burial (Duke and Lewis, 2010). However, the striking difference in color between the Appekunny Formation (dominantly grayish green) and the Grinnell Formation (dominantly red or maroon) is due to the effects of diagenetic fluids, as indicated by both kinds of coloration in the same bed and alternating colors between adjacent beds. Patchy bleaching is also present locally in the Grinnell Formation.

Basin Evolution

The bathymetric evolution of the Belt Basin has been contentious. The Prichard Formation (= Aldridge Formation in southeastern British Columbia) in the Lower Belt consists of turbidites and "hemipelagites" (Cressman, 1989; Ransom and Lydon, 2000). The correlative carbonate platform deposits comprising the Waterton and Altyn Formations in the northeast were deposited mostly in shallow water (Hill and Mountjoy, 1984; Pratt, 1994). The overlying Appekunny Formation and Ravalli Group to the west are dominated by fine-sand–sized sediment and have been considered to record a fluvial environment (Winston and Link, 1993; Winston, 2016). In the east, the lower

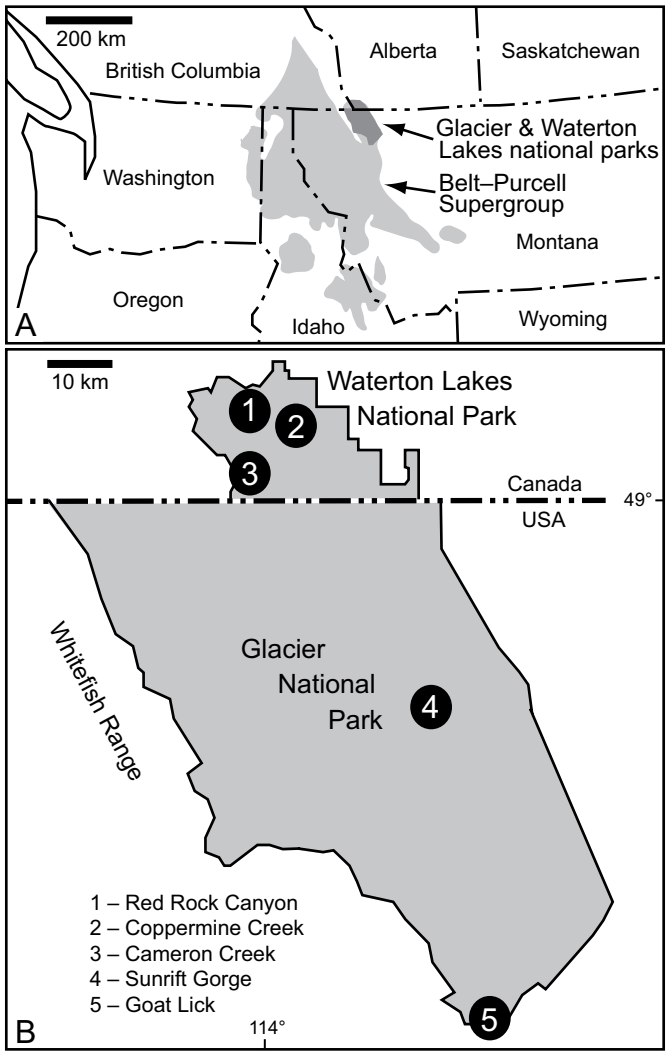

Figure 2. (A) Map of central western North America showing outcrop distribution of Belt Supergroup rocks and Glacier and Waterton Lakes National Parks (Waterton–Glacier International Peace Park astride the border between Montana and Alberta). (B) Map of the national parks showing the locations of measured sections: 1—Red Rock Canyon; 2—Coppermine Creek; 3—Cameron Creek; 4—Sunrift Gorge; 5—Goat Lick. The tourist facility Many Glacier is located between Sunrift Gorge and the international boundary.

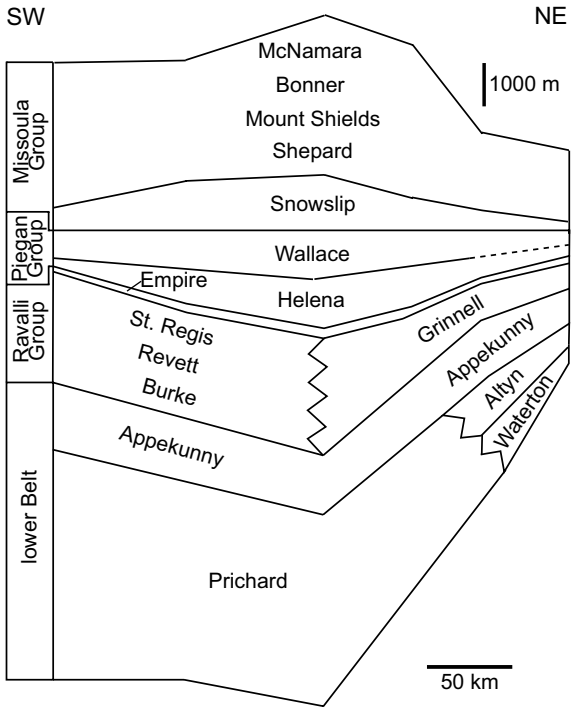

Figure 3. West-to-east-to-north cross section of the Belt Basin from northern Idaho to Glacier National Park in northwestern Montana, showing the main subdivisions of the Belt Supergroup and formations in the lower and middle portion (based on the most recent compilation: Winston, 2016, fig. 1; revised from Winston, 1989a, fig. 3, and Winston, 1990, fig. 5; Winston and Link, 1993, fig. 13). The Wallace Formation was not mapped in Glacier National Park (Whipple, 1992) and directly to the south (Harrison et al., 1996), and the boundary is therefore shown with a dashed line. The Belt Supergroup is called the Purcell Supergroup in Canada, and the formational nomenclature differs somewhat (e.g., McMechan, 1981; Höy et al., 1992; Chandler, 2000).

Appekunny Formation is predominantly argillaceous siltstone to very fine sandstone; plane lamination and rare hummocky cross-stratification (Pratt, 2017) suggest accumulation around storm wave base. The upper part of the Appekunny Formation and the overlying Grinnell Formation are mostly laminated mudstone ("argillite") with ubiquitous "mudcracks." Interbedded quartzose sandstone ("quartzite") has been interpreted as representing subaerially exposed alluvial plains, playas, or tidal flats (e.g., McMechan, 1981; Winston, 1986a, 1986c; Winston and Link, 1993; Chandler, 2000). Herein, we build on an earlier study (Pratt, 1998a) to take a different view that regards the mudcracks as shrinkage-injection features and sedimentation in a permanently submerged, low-energy setting.

Following deposition of green mudstone (argillite) of the Empire Formation, the overlying Helena and Wallace Formations (= Siyeh Formation in southwestern Alberta and Kitchener Formation in southeastern British Columbia) blanketed the basin and do not show a distinct bathymetric polarity other than the restriction of oolite beds and stromatolites to the eastern half (Winston, 2007). Stromatolites indicate deposition within the photic zone. The dominant lithology is laminated, commonly graded argillaceous and silty dolomitic lime mudstone of low-energy aspect, reflecting deposition below storm wave base (Pratt, 2001) rather than in a shallow, intermittently subaerially exposed lake as envisaged by Winston (2007). The succeeding Snowslip Formation of the lower Missoula Group is somewhat similar, but the carbonate content is less (Whipple et al., 1984; Whipple and Johnson, 1988). The Purcell Lava, which was emplaced during deposition of the lower part of the Snowslip Formation in the northeastern region, includes up to 15 m of pillow basalts capped by pahoehoe, suggesting that the basin there was only ~15 m deep at this time (McGimsey, 1985). This argues that the low-energy aspect of most of the units in the northeastern part of the basin was a function of a particularly shallow wave base as a consequence of the semi-enclosed nature of the basin and its limited fetch, along with a paleoclimate that seemingly was not strongly windy or stormy (Pratt, 2001). This would not be unexpected in an equatorial epeiric sea (e.g., Jin et al., 2013). The Bonner Quartzite in the upper Missoula Group is fluvial in origin and derived from south of the basin (Winston et al., 1986), indicating that the basin underwent an episode of subaerial exposure. Otherwise, the rate of erosion of the source area to the west and deposition of mud were essentially balanced by basin subsidence, and a broadly uniform bathymetry was maintained.

GRINNELL FORMATION

The Grinnell Formation was named by Willis (1902). Overall recessive, it is dominated by mudstone (argillite) that is lithologically similar to the mudstone forming the upper part of the Appekunny Formation, except for the presence of interbedded white sandstone (quartzite) and the change from dominantly greenish-gray to dominantly red or maroon color. It was later subdivided into three members, with sandstone more common in the lower and upper units, whereas in the middle member, thin beds of sandstone are a minor component (Fenton and Fenton, 1937). Use of these members has not persisted. Horodyski (1983) and Kuhn (1987) recognized five informal subdivisions. It has been stated that the formation consists of 60% sandstone increasing to nearly 100% in the upper part (Whipple et al., 1984; Whipple, 1992; Harrison et al., 1996), but this has not been encountered in measured sections (Kuhn, 1987; this study), even taking into account the recessive nature of the formation and consequent covered intervals. This study also did not encounter the 400-m-thick sandstone interval at the top of the formation depicted in the generalized stratigraphy at Marias Pass (= Goat Lick herein) by Winston (1989a, fig. 3; 1990, fig. 5; 2016, fig. 1; Winston and Link, 1993, fig. 13; Winston and Sears, 2013, fig. 3). However, the proportion of sandstone decreases rapidly—over a matter of a few kilometers—westward, as well as southward, where the formation passes into the Spokane Formation (Whipple et al., 1984; Earhart et al., 1984; Whipple, 1992; Harrison et al., 1996). For this reason, in western Glacier National Park and the Whitefish Range to the west, the Grinnell Formation can be subdivided into two parts, with sandstone interbedded in the upper part (Whipple et al., 1984). In the Whitefish Range, tabular beds of siltstone and very fine-grained sandstone in the lower part are similar to facies in the equivalent formations farther to the west (Whipple et al., 1984). A similar lithologic pattern is present in the Creston Formation of southeastern British Columbia (McMechan, 1981; Höy, 1992). Sandstone beds are less common and thinner north of Waterton Lakes National Park (Collins and Smith, 1977); the change takes place rapidly, as the difference is apparent just 8 km north-northeast of the Red Rock Canyon section herein.

The formation exhibits south- and southwestward-thickening strata, just 25 km northwest of Waterton Lakes National Park (Collins and Smith, 1977), 225 m to 450 m in Waterton Lakes National Park and just west of it, respectively (Hein and McMechan, 1994), at least 400 m at a location 3 km south of the border and 8 km northwest of Mount Henkel in northeastern Glacier National Park (Ross, 1959), ~600 m on Mount Henkel (Horodyski, 1983), at least 900 m 5 km southeast of Sunrift Gorge (Ross, 1959), 800 m in southern Glacier National Park (Earhart et al., 1984), ~800 m and 1070 m in central-western Glacier National Park and the Whitefish Range to the west, respectively (Ross, 1959; Whipple et al., 1984; Kuhn, 1987; Winston, 1989b, fig. 21; Winston, 1990, fig. 6), and ~1500 m just south of Glacier National Park (Winston, 1989b, fig. 21; Winston, 1990, fig. 6).

Sections were measured at three closely spaced localities in Waterton Lakes National Park and two localities in east-central and southern Glacier National Park, respectively (Figs. 2B and 4–7). These are all on the same Lewis thrust sheet (Whipple, 1992; Stockmal and Fallas, 2015). This thrust represents 140 km of northeastward translation (Price and Sears, 2000; Sears, 2007a).

Composition

The Grinnell Formation consists of mudstone (argillite) and sandstone (quartzite). Mudstone includes laminated claystone, argillaceous siltstone (Fig. 8A), and siltstone (Fig. 8B). Silt is angular and generally well sorted. Detrital muscovite is variably present. In many horizons, the claystone has been eroded into fine sand– to pebble-sized, subangular to rounded, tabular intraclasts ("mud chips") and admixed with silt (Fig. 8C). Sandstone is fine to coarse grained and well sorted, consisting of subrounded to rounded particles; subangular to angular grains are present but fairly rare (Fig. 8D). Small amounts of dolomite occur locally. Pyrite is virtually absent (Slotznick et al., 2016, their table 1).

The clay mineralogy of mudstones is illite and chlorite (Eslinger and Savin, 1973). The illite was generated by burial alteration of smectite (Eslinger and Sellars, 1981). Silt in the Grinnell Formation and correlative units to the west consists of quartz and lesser feldspar, in proportions typically around 3:1 but locally nearly 1:1. The feldspar is primarily albite plagioclase, although K-feldspar is locally present (Eslinger and Savin, 1973; Eslinger and Sellars, 1981). Sandstones consist of quartz with subordinate plagioclase (Ross, 1959).

The mud was sourced from an eroding orogenic belt broadly to the west (Ross and Villeneuve, 2003; Link et al., 2007), whereas the mineralogical differences and zircon ages indicate that the sand came from the low-relief craton to the east (Whipple et al., 1984; Winston,

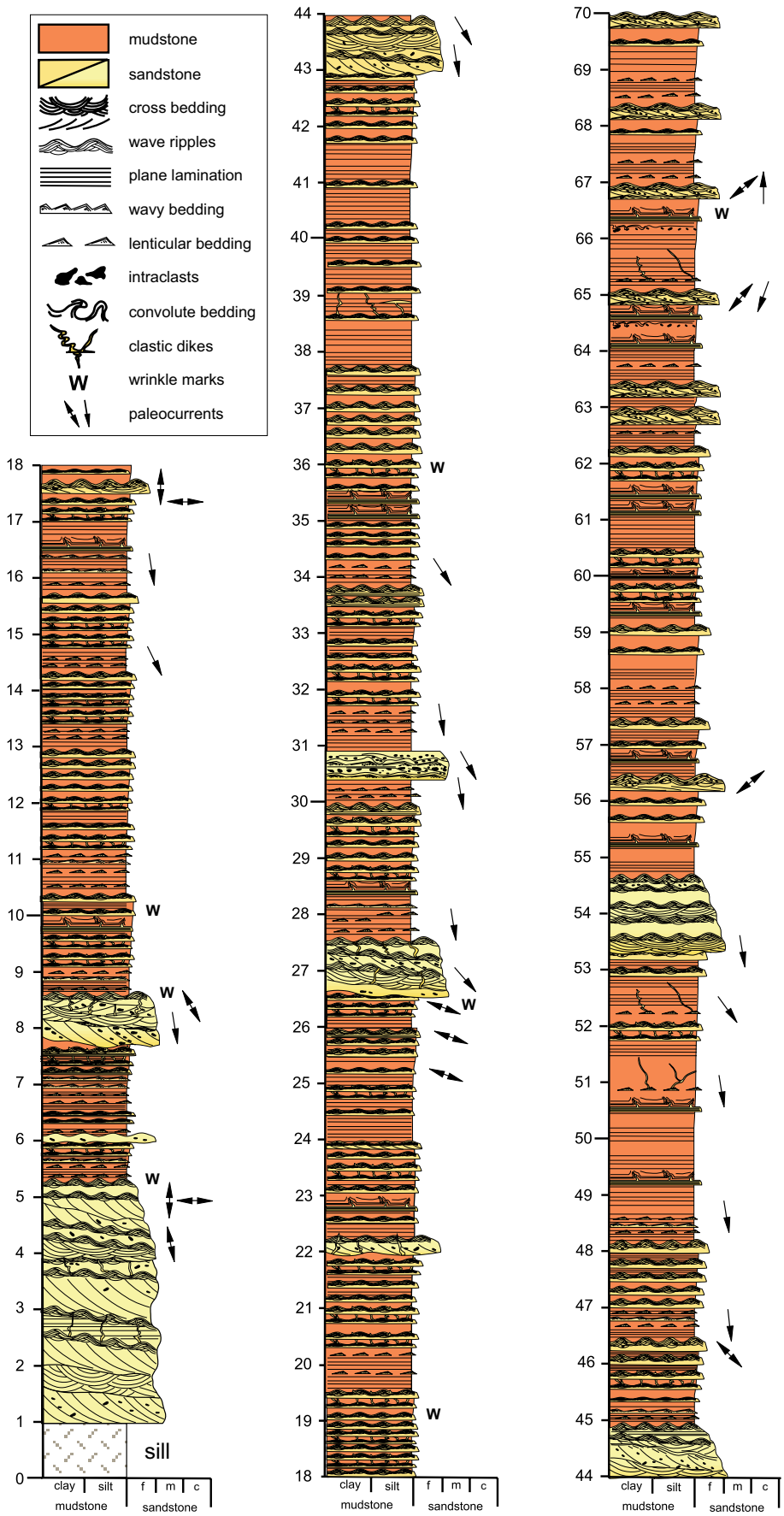

Figure 4. Stratigraphic section (with height in meters) measured in Red Rock Canyon, Waterton Lakes National Park, covering a portion of the lower part of the Grinnell Formation, beginning ~100 m above its base. Section begins at 49°07.771′N, 114°01.709′W and ends at 49°07.894′N, 114°01.602′W. In Figures 5–7, the cross-bedding pattern is diagrammatic and not meant to depict trough cross-bedding; f—fine; m—medium; c—coarse.

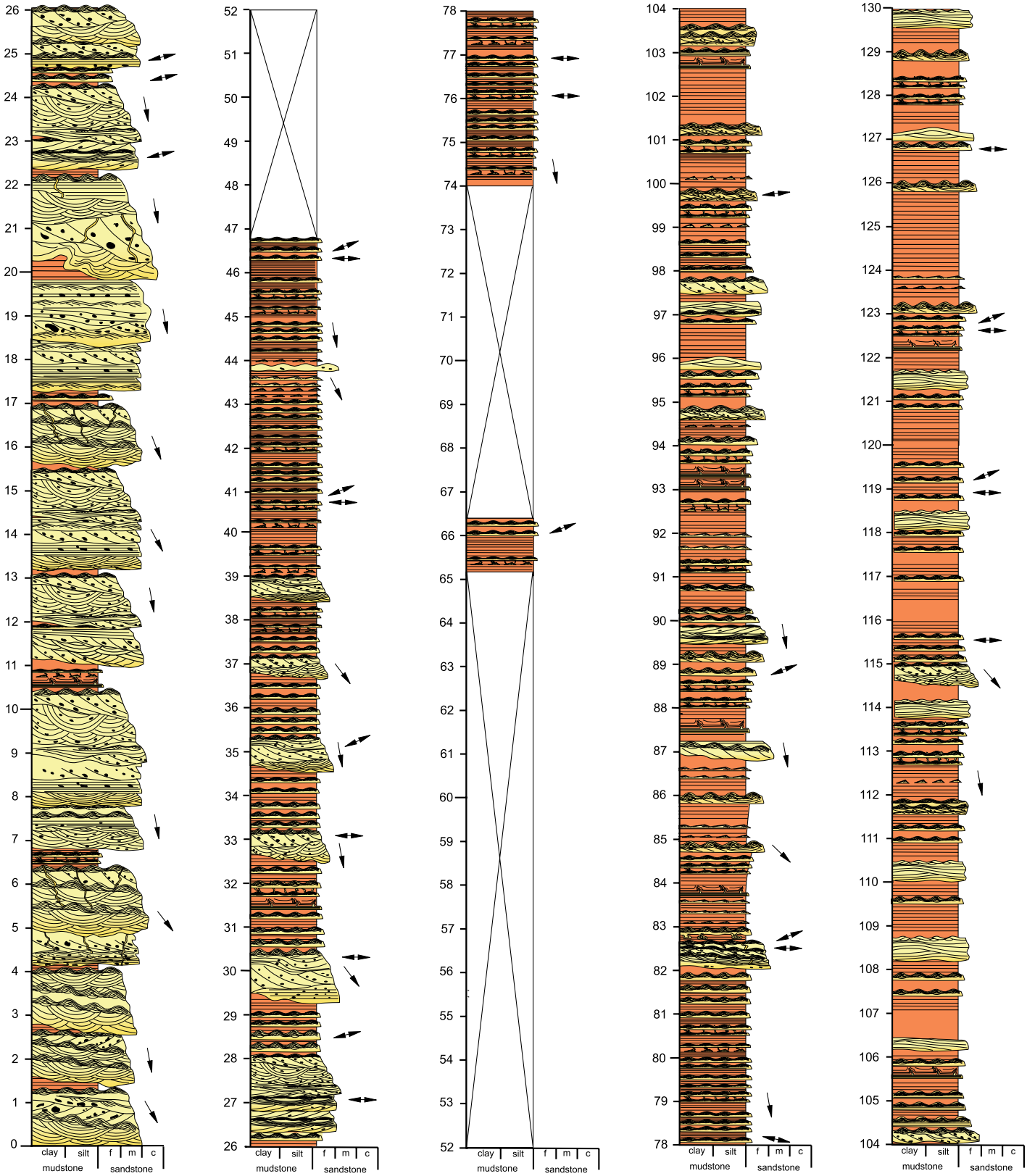

Figure 5. Stratigraphic section (with height in meters) measured on the mountainside by Coppermine Creek on the hillside above Red Rock Parkway, Waterton Lakes National Park, covering a portion of the lower part of the Grinnell Formation, beginning just above its base. Section begins at 49°06.378′N, 113°57.572′W and ends at 49°06.459′N, 113°57.571′W. This section is 5.5 km southeast of Red Rock Canyon. See Figure 4 for legend and abbreviations.

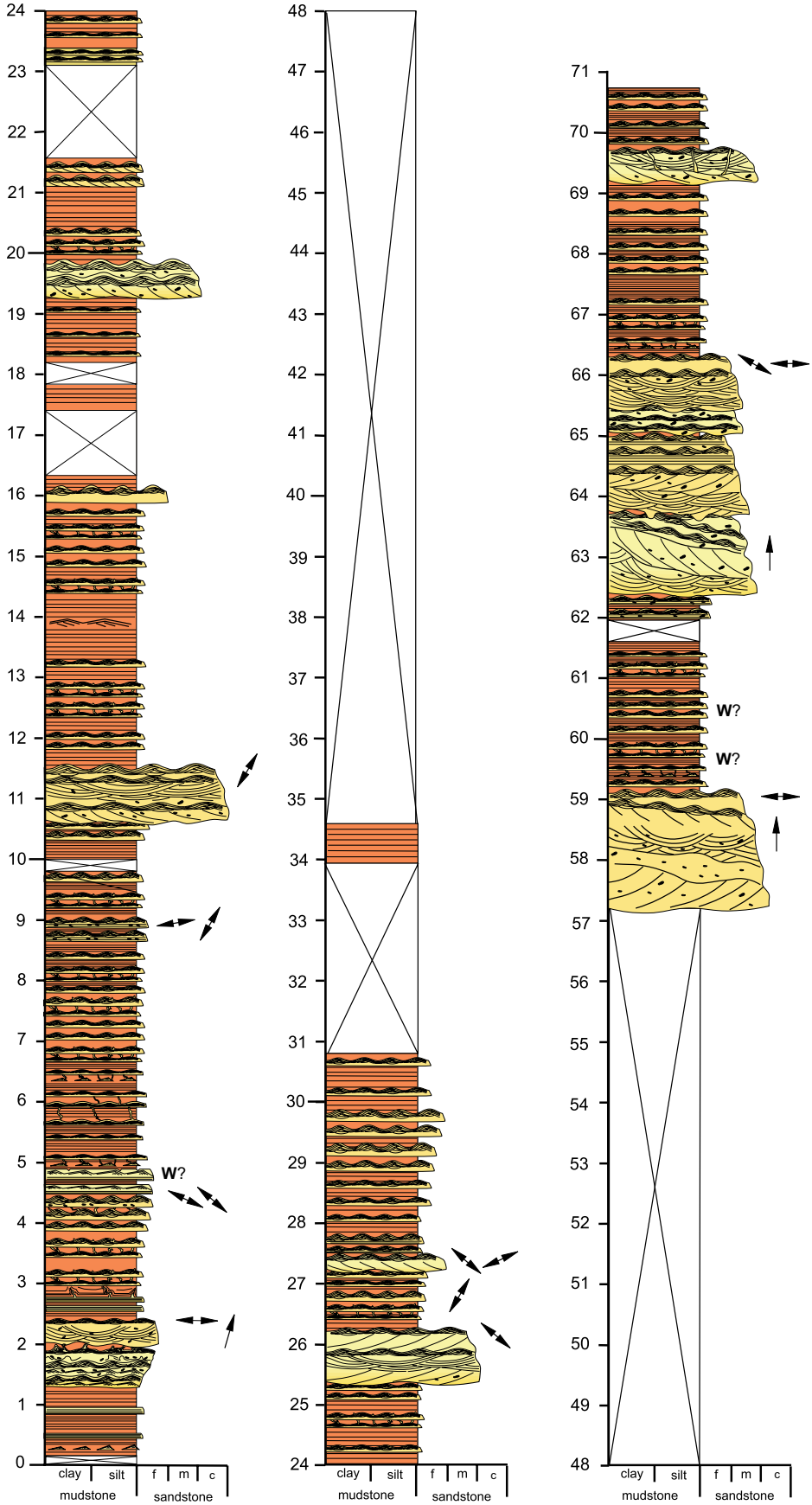

Figure 6. Stratigraphic section (with height in meters) measured on mountainside near Cameron Creek above the Akamina Highway near Rowe Creek, Waterton Lakes National Park, covering a portion of the lower part of the Grinnell Formation, beginning ~100 m above its base. Section begins at 49°03.389′N, 114°00.771′W and ends at 49°03.303′N, 114°00.849′W. This section is 8.5 km south of Red Rock Canyon and 7.5 km southwest of Coppermine Creek.

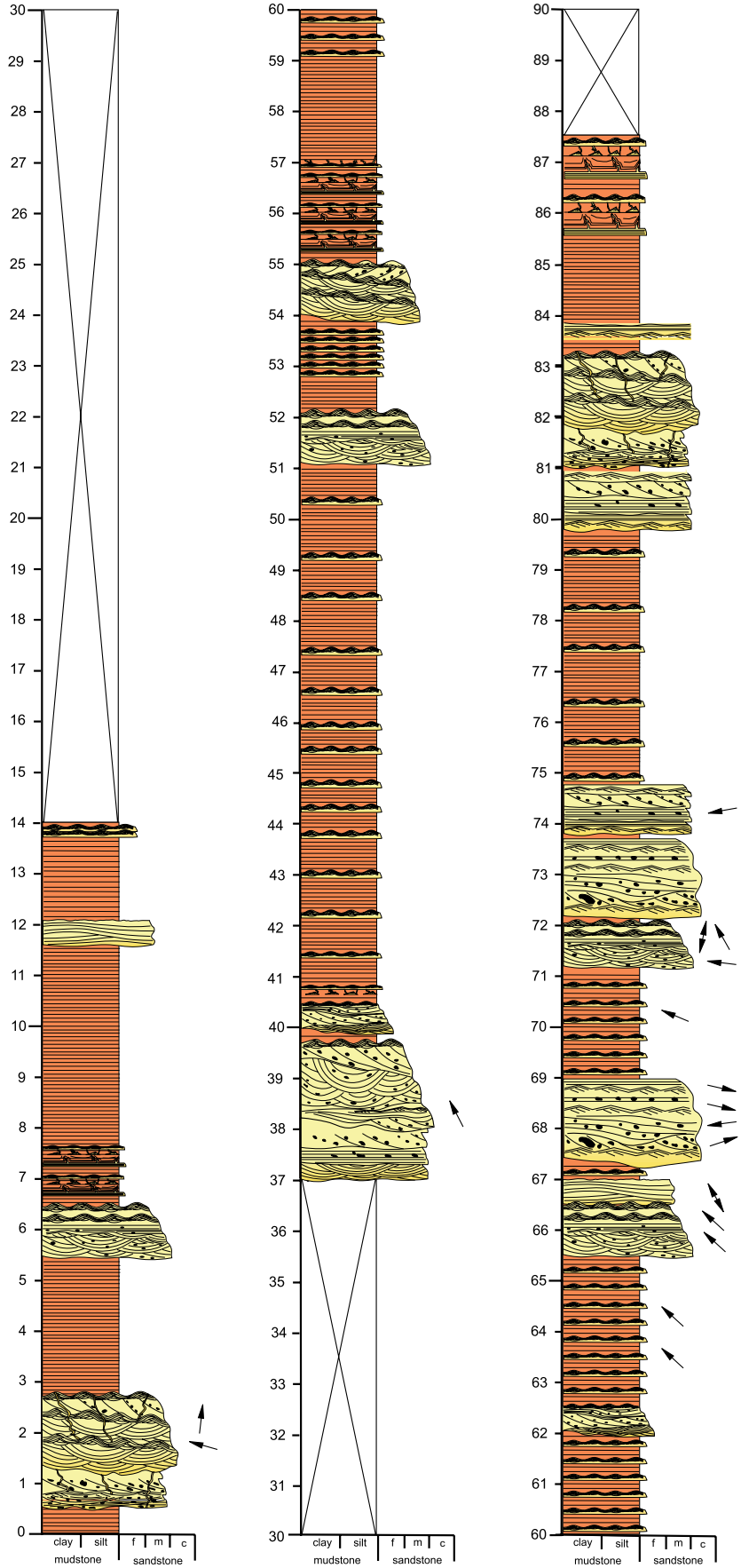

Figure 7. Stratigraphic section (with height in meters) measured in Highway 2 road cut at Goat Lick, southern Glacier National Park, covering a portion of the middle part of the Grinnell Formation. Section begins at 48°15.466′N, 113°34.350′W and ends at 48°15.575′N, 113°34.459′W. Above this is a down-faulted portion of the upper part of the formation, consisting of ~50 m of amalgamated sandstone, followed by ~40 m of decametric intervals of variably interbedded sandstone and mudstone. See Figure 4 for legend and abbreviations.

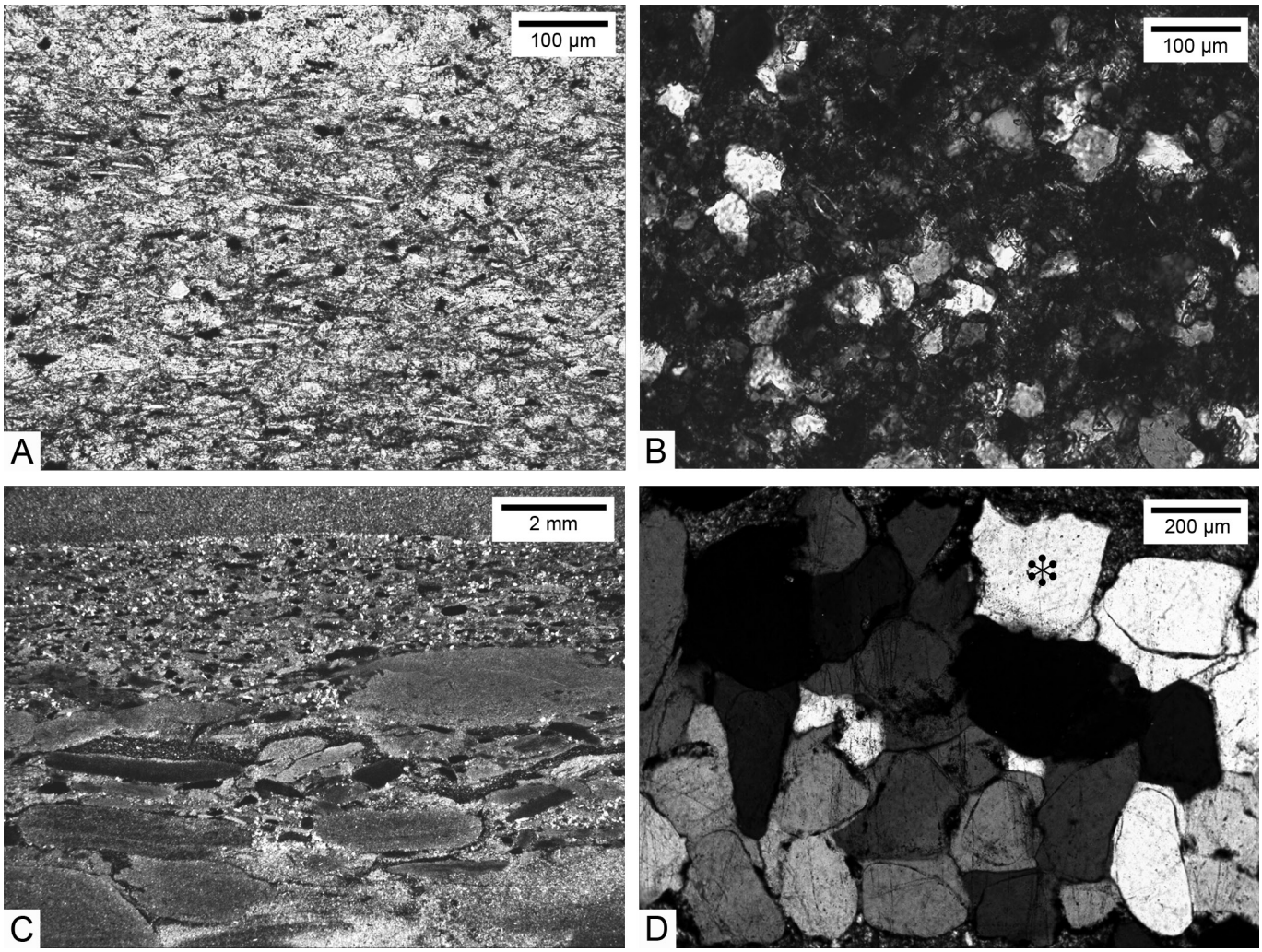

Figure 8. Thin section photomicrographs of sedimentary constituents. A–C are of mudstone (argillite); D is sandstone (quartzite). (A) Angular quartz silt, muscovite, and clay. Plane-polarized light. (B) Angular quartz silt (the outlines are especially clear here because they are surrounded by poikilotopic dolomite cement). Cross-polarized light. (C) Subrounded to rounded, coarse sand- to fine pebble–sized mudstone intraclasts grading upward to very fine-grained sand-sized mudstone grains with quartz silt. Optical scan. (D) Subrounded to rounded fine-grained quartz sand with subordinate angular grains (one is marked with asterisk). Grains at upper right and lower right clearly show quartz overgrowth cement. Crossed-polarized light.

1989b, 2016; Winston and Link, 1993; Pratt, 1998a, 2017; Ross and Villeneuve, 2003). The presence of fresh feldspars is evidence that the sand represents first-cycle detritus (cf., e.g., Tyrrell et al., 2009).

Mudstone (Argillite)

Sedimentary Structures

Although difficult to discern on weathered surfaces, mudstone is planar-laminated with common intraclastic layers. It consists of interlaminated claystone and siltstone, the thicker layers of which are typically normally graded (Figs. 9A and 9B). Siltstone laminae locally have scoured bases (Fig. 9B) and unidirectional cross-lamination, including in lenses representing small starved ripples (Fig. 9C). Tabular claystone intraclasts are oriented parallel to subparallel to bedding (Fig. 9D).

Siltstone beds locally exhibit straight-crested, small-scale symmetrical ripples with wavelengths of 1.5–3 cm, height up to ~0.5 cm, and a ripple index (wavelength divided by height) between 3 and 6 (Figs. 10A–10C). Crests are often flattened (Figs. 10A and 10B). Stratigraphically closely spaced surfaces commonly show contrasting ripple orientations (Fig. 10A). The tops or bottoms of many rippled beds have variably dense populations of halite hopper molds or casts up to ~10 mm across (Figs. 10B and 10C; see also Pratt, 2017, fig. 7F).

Three horizons of dolomitized domical stromatolites have been reported from the lower part of the formation (Rezak, 1957; Horodyski, 1983). These are laterally linked, grading to stacked hemispheroids up to ~30 cm high and 50 cm wide at the base (Fig. 11A). Laminae exhibiting scattered flakes of dolomite intraclasts are present rarely. Upper surfaces of ripples in siltstone sporadically exhibit an "elephant skin" texture, consisting of a fine network of tiny

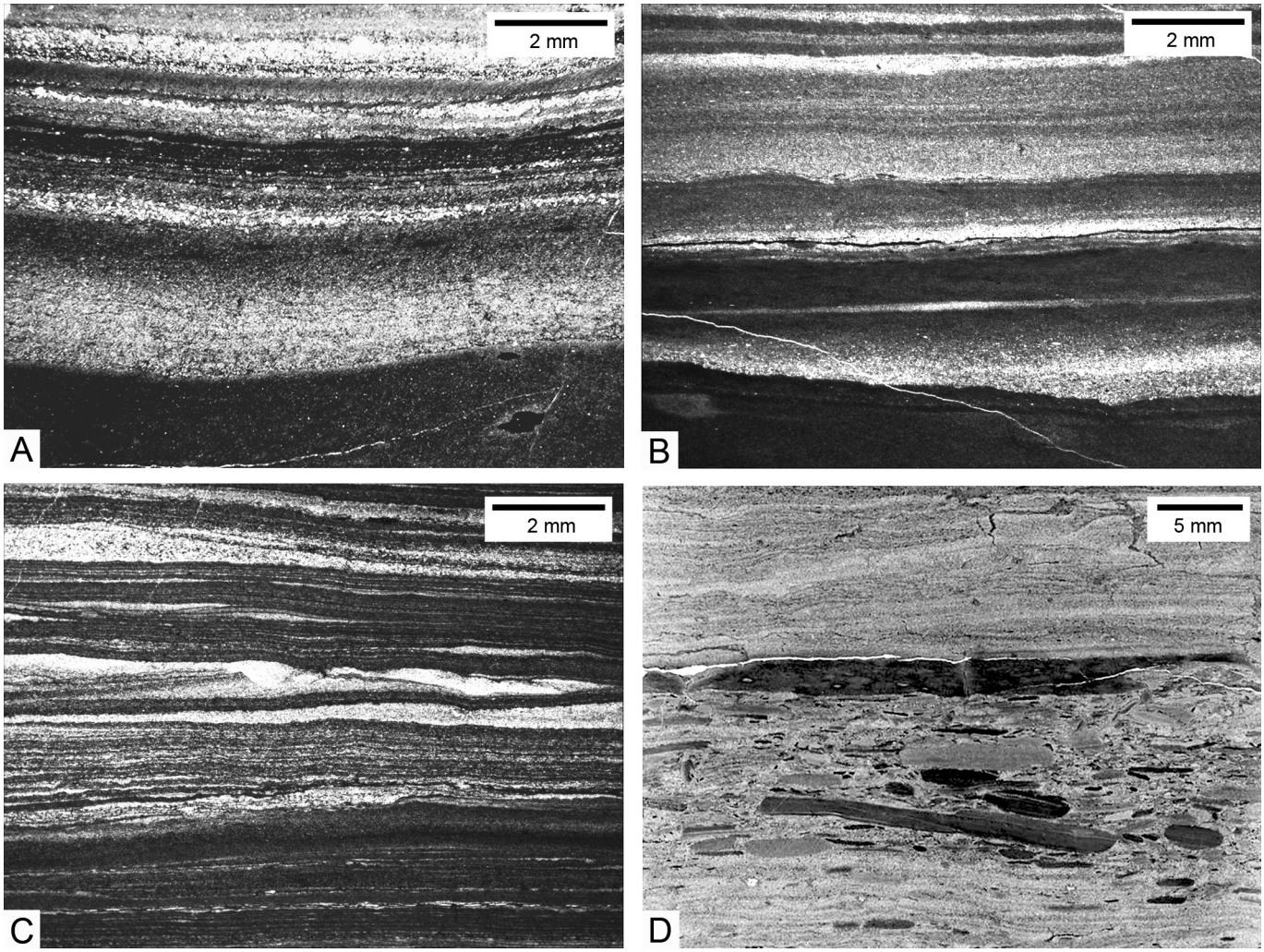

Figure 9. Thin section photomicrographs of mudstone. A–C are under plane-polarized light; D is an optical scan. (A) Interlaminated claystone, siltstone, and graded siltstone. (B) Interlaminated claystone, siltstone, and graded siltstone. Graded layer in lower part exhibits scoured base. (C) Interlaminated claystone, siltstone, and cross-laminated siltstone with starved ripples. (D) Thin bed of claystone intraclasts, in part well rounded, interbedded with plane-laminated siltstone.

ridges, less than 1 mm high (Fig. 11B). These exhibit a weak linearity. By contrast, wrinkle marks of *Kinneyia* type are relatively common on upper surfaces (Fig. 11C). Rare upper and lower surfaces exhibit scattered small pits and casts, respectively, several millimeters wide.

Soft-Sediment Deformation

Synsedimentary deformation is pervasive in the mudstone facies. In many intervals, laminae are crinkled to gently undulating, and bed surfaces are creased or lumpy. Most bedding planes exhibit distinctive crack arrays that include polygonal, orthogonal, straight linear, curving linear, and spindle-shaped patterns (Figs. 12A–12I; also Pratt, 2017, fig. 7E). Polygons are not uniform on each surface and range in diameter from a few centimeters up to ~20 cm. Where not joining other cracks, crack terminations taper to a point. Two sizes of crack systems are common in that small arrays may be present in the polygons formed by larger cracks. Where cracks and halite crystal casts occur, the cracks crosscut them.

In vertical section, cracks are vertically to obliquely oriented and straight to undulating to branching, and they are from less than one to several millimeters up to more than a centimeter wide, and a few millimeters to 10 cm long (Figs. 13A–13E and 14A–14E). Crack margins are variably cuspate, and they are parallel-sided to downward tapering. Claystone laminae commonly become gradually slightly thinner away from silty crack fills, losing up to about one third their thickness.

Cracks are filled with variable amounts of clay and silt, plus intraclasts exhibiting various orientations from subparallel to bedding to steeply inclined, as well as sand if the crack intersects a sandy lamina. This material is typically traceable to underlying laminae and therefore was ejected a short distance laterally and emplaced in a upward direction. There is no evidence for gravitational infilling from above, such as geopetal layering. Crack fills and host laminae are locally distorted by folding and shearing (Figs. 13A and 13B). In one example, a gutter crosscuts prior-formed cracks, as well as being penetrated by reactivated cracks from below (Fig. 13E).

Many crack arrays involve disruption and brecciation whereby claystone laminae are

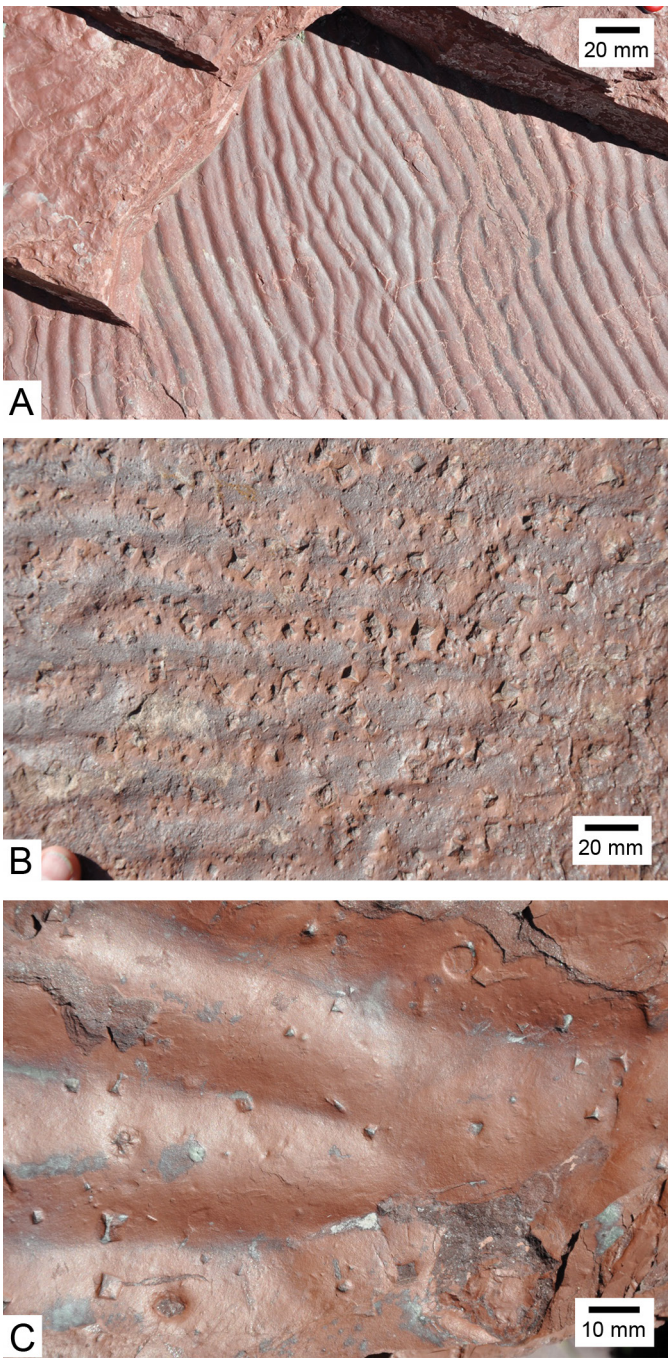

Figure 10. Sedimentary features in mudstone. (A) Underside of beds showing two sets of straight-crested symmetrical ripples. (B) Top of bed showing straight-crested, low-amplitude symmetrical ripples and abundant halite hopper crystal molds. (C) Underside of bed showing straight-crested symmetrical ripples and scattered halite hopper crystal casts.

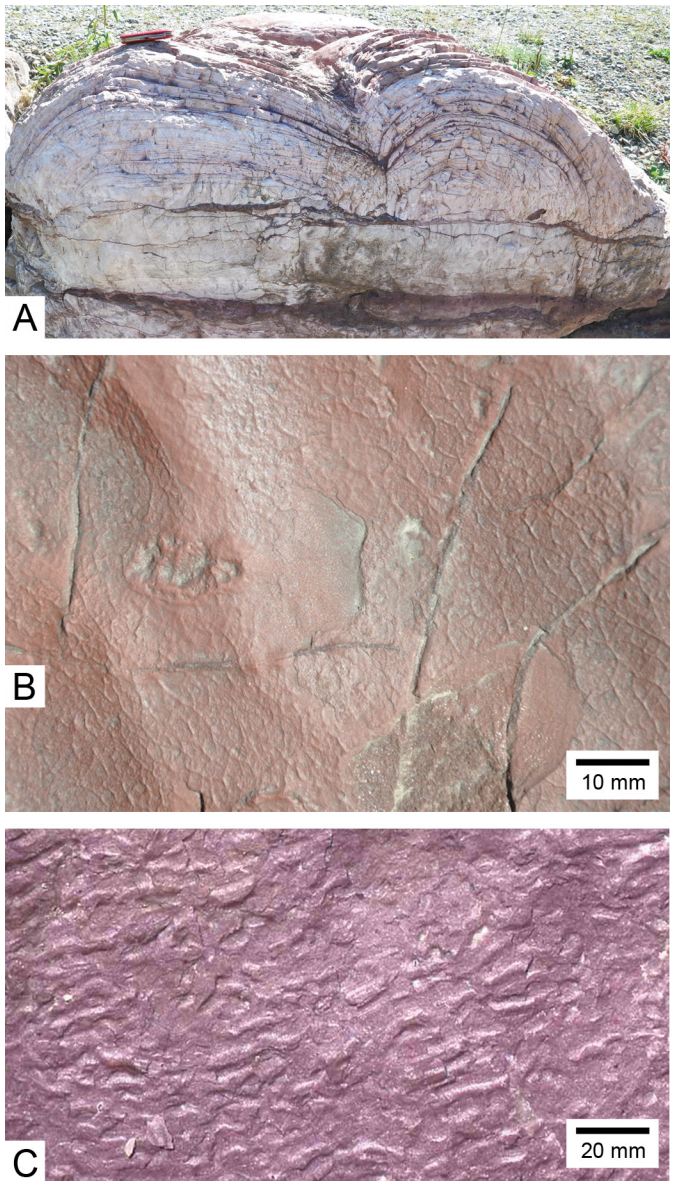

Figure 11. Microbial and hypothetically microbial sedimentary features. (A) Thin dolomite bed passing upward into laterally linked hemispheroidal stromatolites. Red Rock Point, western side of Glacier National Park. Pocket knife is 8.5 cm long. (B) Top of mudstone bed showing straight-crested to gently undulating symmetrical ripples with fine network of tiny ridges less than 1 mm in height ("elephant skin"), with a dominant upper-left to lower-right orientation (cut later by discontinuously interconnected dikes sourced from underlying layer). This is a close-up of the surface shown in Figure 13H. (C) Top of mudstone bed showing *Kinneyia*-type wrinkle marks.

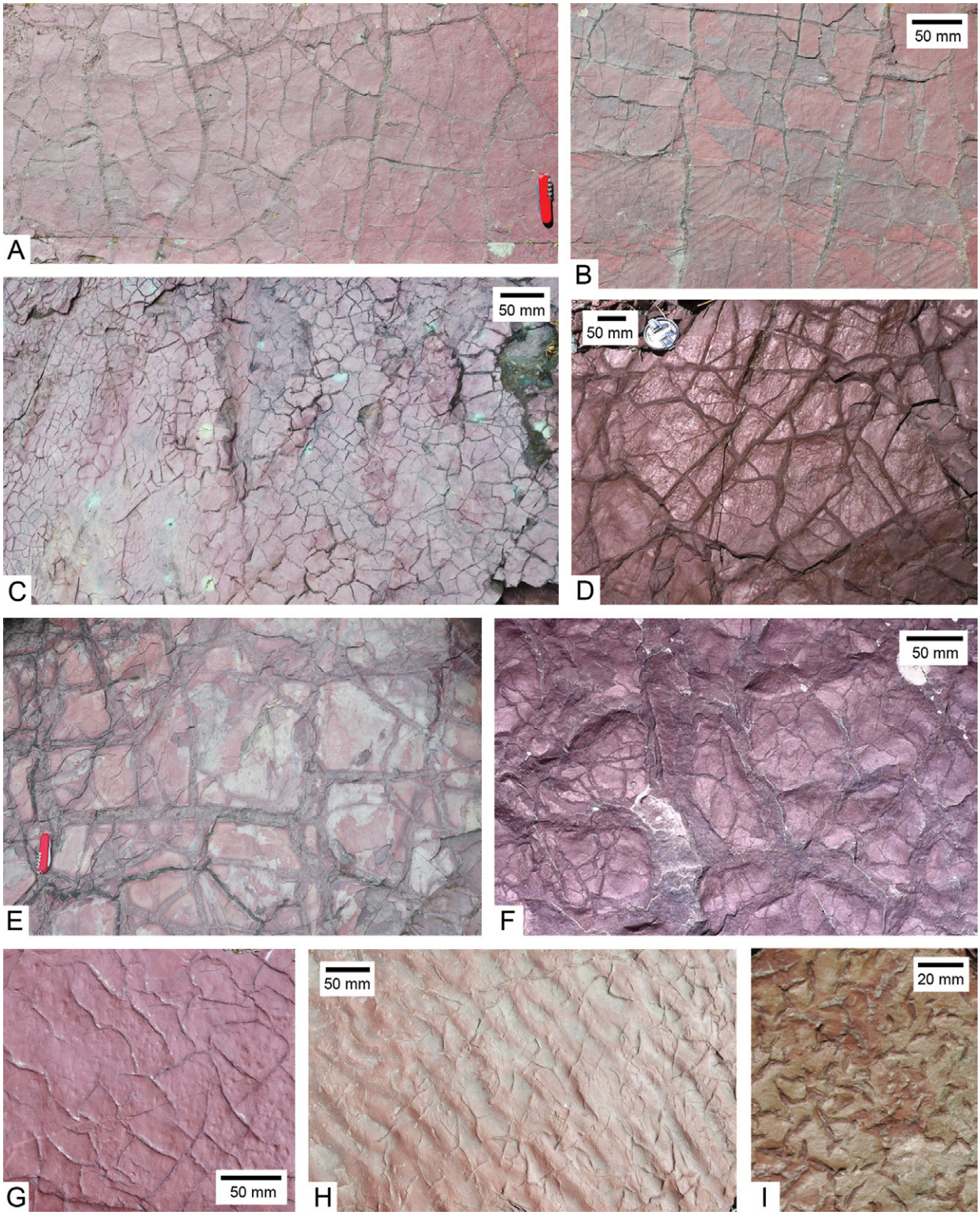

Figure 12. Bedding plane views of crack systems cutting mudstones (and their fills, i.e., small dikes). (A) Reticulate pattern formed by long, straight, and gently curving cracks. (B) Reticulate pattern of long, crudely rectilinear cracks penetrating surface with straight-crested, short-wavelength, low-amplitude ripples. (C) Irregular polygonal pattern formed by interconnected short cracks. (D) Irregular polygonal pattern formed by interconnected short cracks with subordinate narrow cracks. (E) Crudely rectilinear pattern formed by wide cracks. (F) Irregular polygonal pattern formed by wide cracks with subordinate narrow cracks. (G) Incomplete polygonal pattern formed by short curving cracks. (H) Intersecting, discontinuous short cracks cutting oscillation ripples. (I) Intersecting, short spindle-shaped cracks. Pocket knife in A and E is 8.5 cm long.

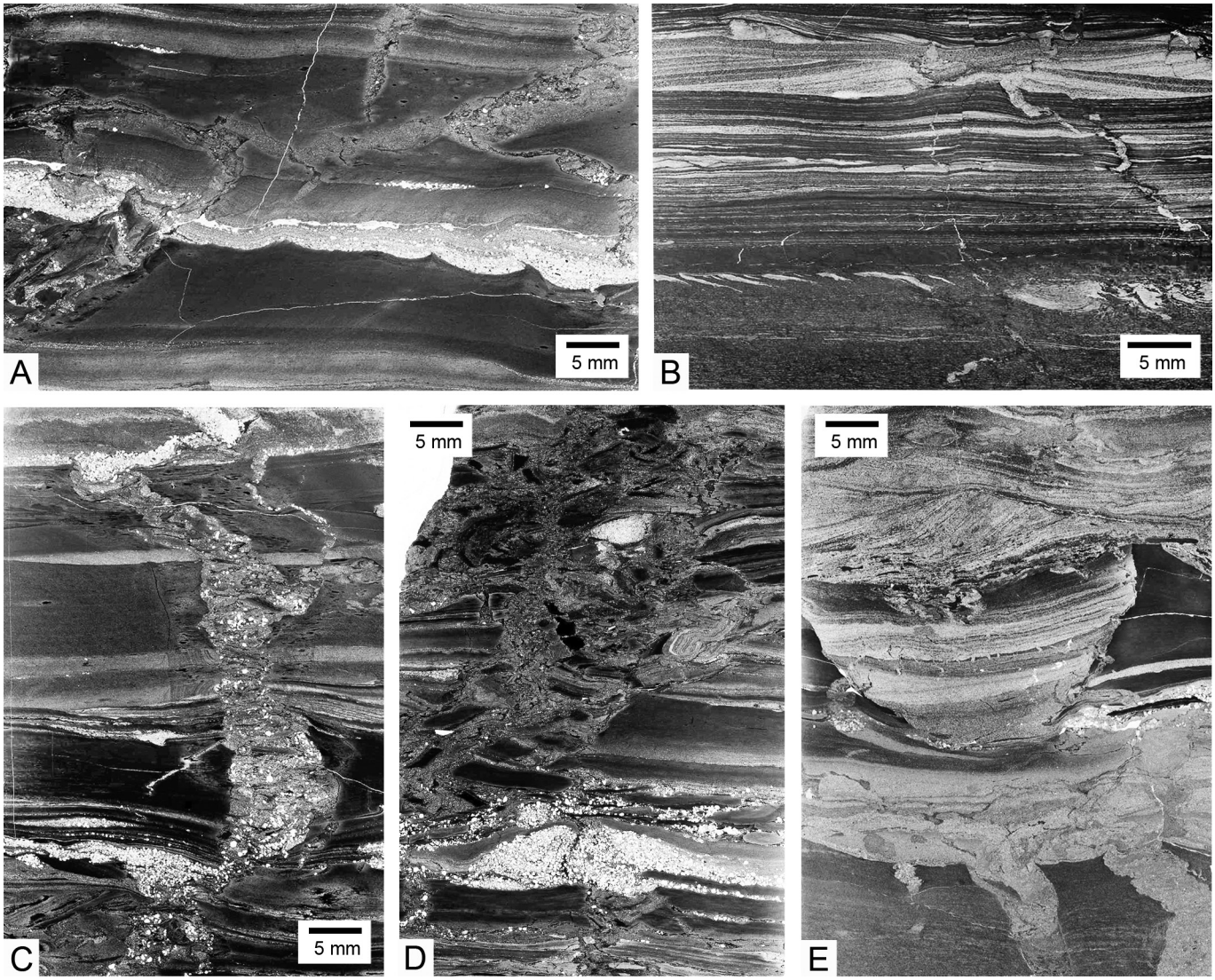

Figure 13. Optical scans of thin sections of sediment-filled dikes crossing mudstone consisting of claystone, siltstone, and sandstone laminae. Darkest laminae are claystone; grayish laminae are siltstone; lightest laminae and grains are sandstone. Scale bar is the same for B–D. (A) Obliquely oriented branching dike system containing variable amounts of clay, silt, and sand, and mudstone intraclasts at lower left. Base of sandstone lamina exhibits flame structures. (B) Obliquely oriented, silt-filled dike (right), several squashed dikes, and a lamina (one-third from bottom) containing sheared, small silt-filled dikes. (C) Wide vertical dike with smaller branches containing clay, silt, and intraclasts. In lower left, mudstone laminae and small dikes are convoluted. (D) Wide vertical dike with smaller dikes in lower part, filled with clay, silt, sand, and abundant intraclasts (breccia-like). Some mudstone fragments are folded (e.g., center-right). (E) Silt-filled dikes in lower part, in turn overlain by gutter cast containing small dikes at different levels and rippled very fine-grained sandstone.

fractured and separated both across and parallel to the layering (Figs. 14A–14E). Laminae and breccia fragments are often gently folded, fractured, or displaced after formation. Crack margins are flat and parallel-sided to cuspate. Many or most intraclastic horizons are closely associated with brecciation, in that fragments have been reworked into intraclasts by currents (Figs. 14C and 14D). Oblique cracks locally resulted in the generation of larger blocky intraclasts (Fig. 14E).

Sandstone (Quartzite)

Sedimentary Structures

Sandstones range from lenticular, to undulating, to tabular thick laminae and thin to medium beds to broadly tabular thick beds variably intercalated in mudstone successions (Figs. 15A, 15B, 16A–16F, and 17). Lateral change of thickness is due to both erosional bases as well as topography of bed forms and composite bar forms (Figs. 15B, 16A, and 16B). Sandstones have sharp, erosive bases, locally forming gutter-like casts several to tens of centimeters wide and up to 4 cm deep (Figs. 18A and 18B). Large-scale planar, concave-up, and sigmoidal cross-lamination is present in thin to medium beds (Figs. 15A, 15B, 16A–16D, and 19A–19C; see also Pratt, 2017, fig. 7B); trough cross-bedding appears to be absent. Hummocky cross-stratification also appears to be absent, but the cross-lamination in some beds locally

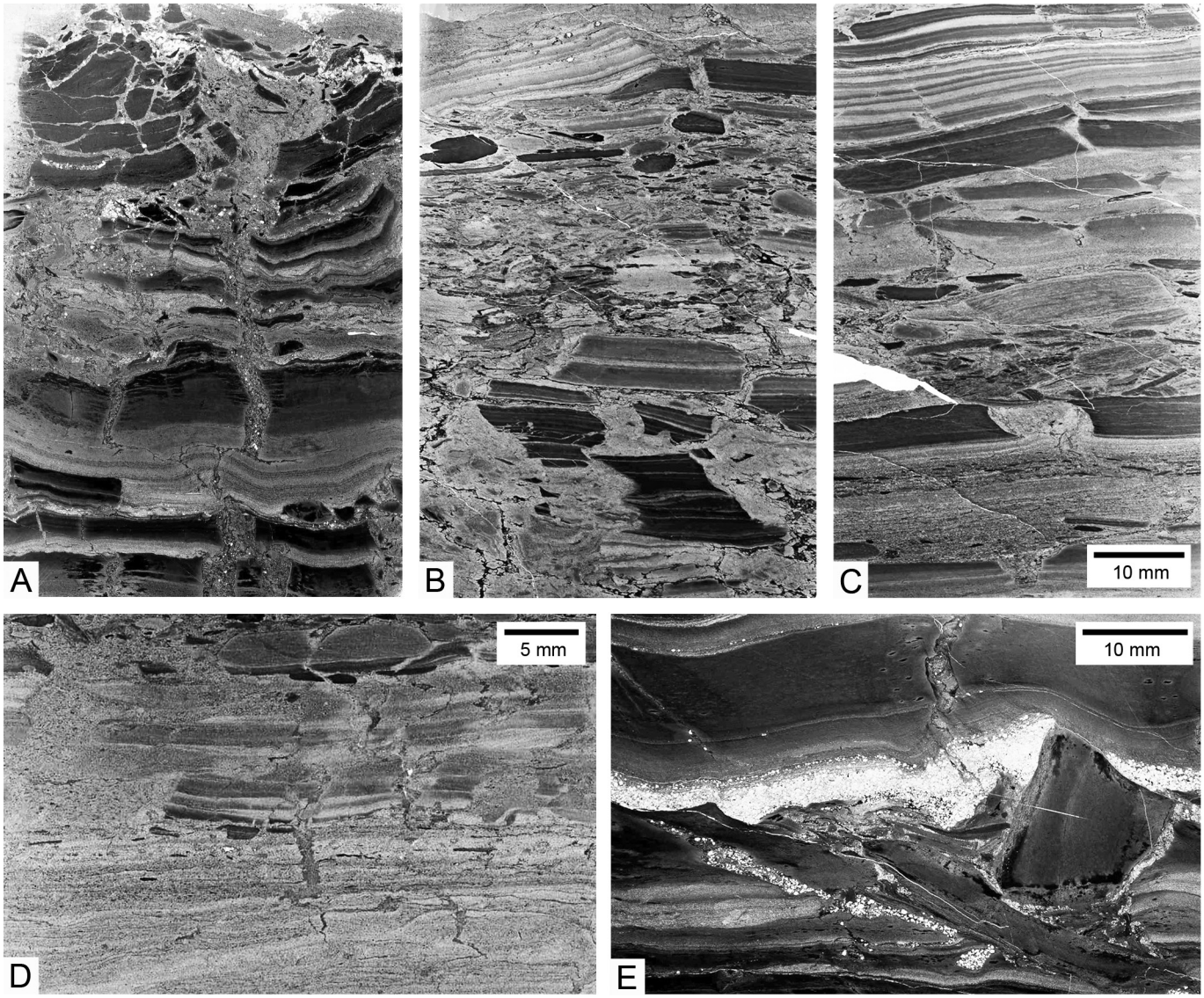

Figure 14. Sediment-filled dikes crossing mudstone leading to various degrees of intrastratal disruption and brecciation. A–C and E are optical scans; D is under plane-polarized light. Scale bar is the same for A–C. (A) Mudstone laminae disrupted in lower part and brecciated in upper part. (B) Mudstone laminae brecciated with possible current reworking and rounding above the middle part. (C) Mudstone laminae disrupted in lower and upper part, and brecciation in the middle part with possible current reworking and rounding. (D) Subrounded to subangular, blocky to tabular claystone intraclasts in laminated mudstone with small cracks. (E) Intrastratally deformed interval showing folded lamination, sand injection, disrupted laminar claystone intraclasts, and large, tilted, angular, blocky intraclast.

approaches swaley shapes (Figs. 16E, 16F, 19A, and 19B). The tops of some thin beds exhibit two-dimensional symmetrical ripples with wavelengths of ~5–15 cm, heights up to 3 cm, and a ripple index of up to 5 (Fig. 19C). More commonly, thicker intervals exhibit two-dimensional symmetrical ripples with ~10–20 cm wavelengths and a ripple index of around 8–10 (Figs. 20A–20C). Crests are relatively straight or undulate at the meter scale, and, in places, there are sets of smaller two-dimensional symmetric ripples in the troughs oriented at right angles or oblique to the larger crests ("ladder-backed ripples"). Three-dimensional ripples occur rarely.

Amalgamated thin and medium beds commonly form thick beds and massive intervals (Figs. 19A–19C). Discontinuous mudstone laminae may be intercalated. Internal scour surfaces are locally present, and in many cases, it is not possible to separate individual beds. Unidirectional cross-lamination shows variable and even reversed directions in adjacent layers (Figs. 16A–16D, 19A, and 19B).

Granule- to medium pebble–sized mudstone intraclasts are almost everywhere incorporated in the sandstone (Fig. 21A). They are dominantly tabular, but lenticular and blocky shapes are common, and they are subangular to subrounded (Figs. 21B–21D). In some beds, there are large rounded clasts of agglomerated sand, mud, and small intraclasts, sometimes with an intraclast core (Fig. 21E). In some cases, sand

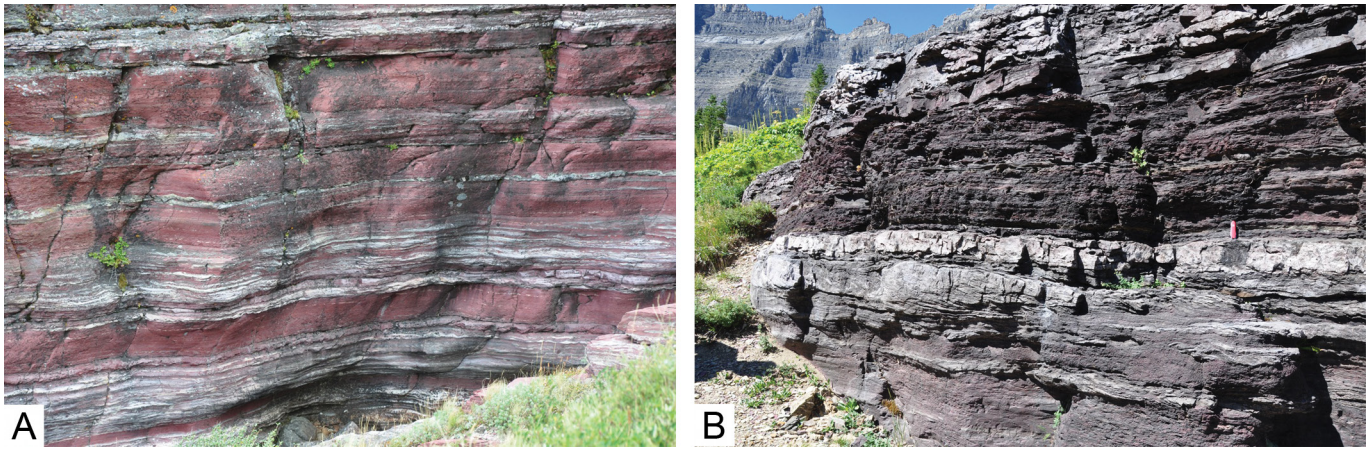

Figure 15. Outcrops of red mudstone (argillite) with interbedded white sandstone (quartzite). (A) Approximately 5-m-high cliff from the middle part of the formation, showing tabular and lenticular sandstone beds. Baring Creek north of Sunrift Gorge. (B) Cliff from upper part of the formation, showing tabular and lenticular beds of sandstone. Ptarmigan trail northwest of Many Glacier. Pocket knife (center-right) is 8.5 cm long.

may be concentrated around the periphery (Fig. 21F), forming an "armored mud ball."

Despite the variable ripple orientation on some individual bedding surfaces, paleocurrent measurements from unidirectional cross-lamination and symmetrical ripples (Fig. 22) suggest a southerly to southeasterly flow direction for the lower part of the formation, with a northerly to northeasterly component for the former, and common west-east and northwest-southeast oscillatory flow directions for the latter. The middle part of the formation at Goat Lick, at the southern side of Glacier National Park, shows a westerly to northwesterly flow direction. The number of measurements at Cameron Creek and Goat Lick did not give a dominant flow direction. Paleocurrents measured in the upper Creston Formation in southeastern British Columbia are similarly variable, with a dominance of broadly westerly and easterly flow directions (McMechan, 1981).

Soft-Sediment Deformation

Synsedimentary deformation is pervasive in the sandstones as well. In places, individual thin beds show gentle folding. Common features are short sand-filled cracks, occurring as dike arrays projecting from either the bed sole or bed top or both (Figs. 23A–23D; see also Pratt, 2017, fig. 7C). In plan view, these form polygonal, densely interconnected spindle shapes, isolated linear segments, or networks dominated by sinusoidal patterns. The last style occurs on some bed tops in symmetrical ripple troughs and conforms to the sinusoidal pseudofossil *Manchuriophycus* (Fig. 23B). Dike width varies from <1 mm to ~10 mm, and in places, there are two crude size groupings (Fig. 23C).

In cross section, dikes extending from bed upper surfaces tend to be relatively straight (Figs. 24A and 24B). Those projecting from bed soles, however, are ptygmatically folded and commonly obliquely oriented, and they can reach up to 20 mm in length, or more if unfolded (Figs. 24C and 24D). Sand grains in the dikes are in grain-to-grain contact, but locally with admixed mud. In some cases, silt- and clay-filled cracks in mudstone are crosscut by a later generation of dikes (Fig. 24E). In other cases, muddy, intraclastic crack fills emanating from underlying mudstone penetrate the bottoms of sandstone beds (Fig. 24F).

INTERPRETATION

Deposition

Mudstone (Argillite)

Mudstone represents background sedimentation. The predominance of plane lamination and the absence of large-scale scours suggest deposition below fair-weather wave base. The great thickness of the formation with no perceptible differences or unconformities indicates an equilibrium in which a more or less constant bathymetry was maintained. The relative abundance of feldspar in the silt argues that the orogenic source region to the west was probably semiarid. Halite molds and casts are evidence that the climate of the Belt Basin was arid. The submerged depositional setting and absence of evidence for gypsum mean that halite had to have precipitated out of bottom-hugging brines that were concentrated elsewhere, presumably in playa-like lagoons and sabkhas in low-relief coastal areas broadly to the east. The casts suggest that the halite was dissolved at or just under the sediment-water interface when the pycnocline disappeared as salinity reverted to more normal marine conditions. This is supported by some surfaces with small dikes that crosscut the casts after formation. Density stratification in the basin may have developed more often than what is indicated by the numerous bedding planes with halite, but salinity might not have been high enough to lead to precipitation.

Graded bedding and local asymmetric ripples in the silty laminae suggest these are distal turbidites with thin upper-T_C, T_D, and $T_{E–I}$ divisions from low-density gravity flows (e.g., Talling et al., 2012) derived from sources broadly to the west. Presumably, the bulk of the sediment from these flows was deposited in more proximal areas. Planar claystone laminae were probably deposited by hemipelagic settling from hypopycnal plumes from the same source region.

Small symmetrical ripples in siltstones were formed by wave action that resuspended muds after deposition. Small wave orbitals formed by short-period, wind-driven waves generate steep-sided vortex ripples with short wavelengths (e.g., Clifton and Dingler, 1984; Wiberg and Harris, 1994). These are typical of very shallow bays and lakes with limited fetch and are common in many lacustrine successions (e.g., Allen, 1981; Aspler et al., 1994). The small wave ripples in the Grinnell Formation, however, developed in mud. They were probably produced in somewhat deeper water by longer-period waves when the flow velocity was large enough for

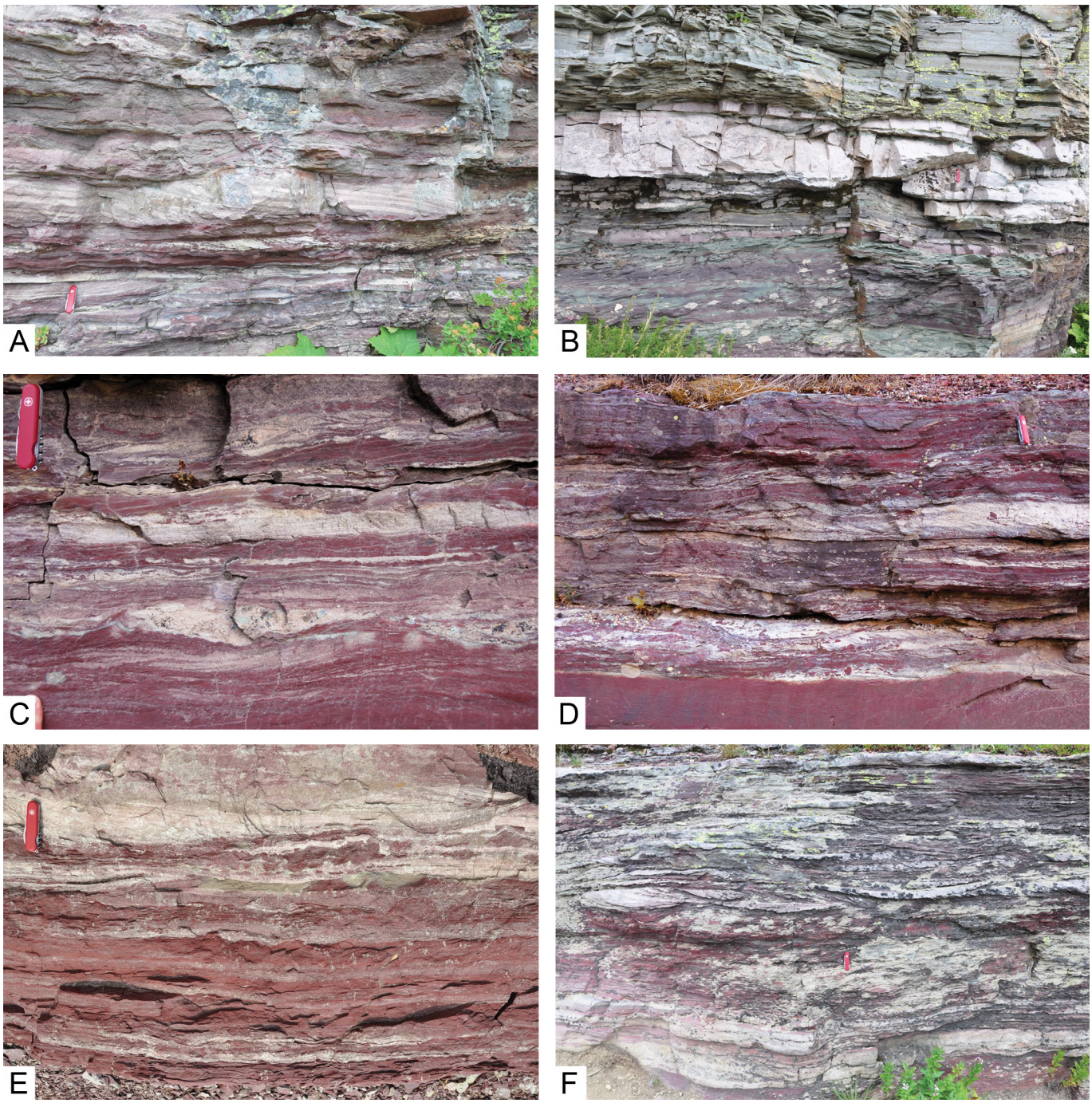

Figure 16. Interbedded sandstone and mudstone. (A) Thin sandstone beds with lenticular medium bed showing roughly eastward-directed planar cross-lamination. Grinnell Glacier trail southwest of Many Glacier. (B) Thin sandstone beds with two overlapping lenticular beds with opposing cross-lamination. Grinnell Glacier trail. (C) Thin sandstone beds showing plane-lamination, eastward- and westward-directed cross-lamination, and minor swaley cross-lamination. Sunrift Gorge. (D) Thin sandstone beds with sharp or scoured bases showing dominantly eastward-directed and subordinate westward-directed cross-lamination; mudstone intraclasts are common. Sunrift Gorge. (E) Thin sandstone bed (at pocket knife) with a swaley shape, overlain (at right) by eastward-directed cross-laminated lens. Goat Lick. (F) Thin sandstone beds with lenses showing opposing cross-lamination and a swaley feature (middle). Grinnell Glacier trail. Pocket knife is 8.5 cm long.

grain movement. The wave action could have been from occasional storms.

Variably common intraclastic layers indicate frequent events of bottom scour and rounding by wave action, at and near the limit of storm wave base. The absence of intraclast imbrication is evidence that the resulting oscillatory currents were generally weak. The poor sorting and rarity of layers of sand-sized intraclasts also suggest that reworking was not protracted or repeated, as would be expected within fair-weather wave base. In many such horizons, erosion was preceded and thus assisted by prior crack formation and disruption. This is explored further below. Intraclastic layers have a stratigraphic frequency broadly at the decimetric scale, so their formation was a not seasonal or annual meteorological phenomenon.

Storm wave base was probably relatively shallow. In a fully developed sea, wave base (wavelength divided by two) for deep-water waves with a wavelength of 40 m and wave height of 1.8 m, produced by 40 km/h winds with a fetch of ~150 km, is ~20 m, i.e., twice that from 30 km/h winds (e.g., Trujillo and Thurman, 2017, chapter 8). The stromatolitic levels corroborate deposition within the photic zone; *Kinneyia* wrinkle structures and "elephant skin" textures—if these were microbially induced—support this. It is also possible that density stratification may have reduced storm wave base. The rare surfaces with pits may be the same structures stated to be raindrop and hail imprints by Kuhn (1987), but the small size, shape, absence of raised rims, and lack of overlap are not typical (e.g., Uchman et al., 2004; Rindsberg, 2005).

Balls of agglomerated mud, sand, and intraclasts suggest that the clayey sediment was initially sticky. However, intraclasts, cracks, disruption, and bending indicate that soon after deposition, the mud layers possessed a rheology that ranged from ductile to stiff. There is no evidence that it was loose and fluffy or formed a dense suspension ("fluid mud"). Length of ptygmatically folded dikes versus sediment thickness below sandstone beds suggests a water content of the mud up to ~70% when sand was injected. In some instances, however, thinning away from crack fills suggests a water content of up to ~30%, but planar laminae and intraclasts indicate it was typically much less. Burial compaction effects appear to be minimal, because folding of dikes was mostly due to the deformation event itself, and blocky intraclasts are not distorted. Flocculation and cohesiveness were enhanced by electrostatic attraction due to the marine salinity, although clays do not appear to have formed large floccules in the water column. This implies that suspended and settled organic matter played little to no role, and whatever might have been in the water column and attached to clays was rapidly oxidized. In turn, this suggests biological productivity was low overall. Frequent small earthquakes may have caused edge-to-edge orientations to collapse and expel their pore water, thereby mimicking burial effects.

Sandstone (Quartzite)

The absence of gradational transitions between mudstone and sandstone intervals indicates that the sands punctuate background mud deposition and are not evidence for episodic deltaic input, river flooding, or regional bathymetric changes such as shallowing events. A source from the reworking of eolian dunes on the adjacent land surface is considered unlikely given the lack of evidence for strong winds and wave action. Rather than consisting of sediment delivered directly from fluvial sources, the dominantly rounded nature of the sand grains is evidence that they were subjected to protracted wave action, in sand bars and on beaches, before being transported into deeper water.

Cross-lamination from large current ripples indicates unidirectional flow of ~0.3 m s^{-1}. However, the common presence of scoured bases and muddy intraclasts, and the lateral thickness changes suggest that the consolidated muddy seafloor, as well as previously deposited sand, may have been eroded by bottom currents that were stronger initially, perhaps exceeding 0.5 m s^{-1}. Sporadically occurring swaley bedding is evidence that combined flows occasionally developed. Symmetrical ripples, especially on bed tops, indicate that the final regime was oscillatory flow from wave action, occasionally followed by weaker oscillatory flow at right angles or oblique to the previous current direction, which produced smaller ripples in the troughs. These attributes along with the absence of hummocky cross-stratification and other strong storm-generated effects argue that the sandstone beds are not tempestites.

Given the low-energy aspect of the mudstone, strong bottom scour and transport of relatively well-sorted coastal and nearshore sands are interpreted to be due to a combination of tsunami-induced processes, including: (1) onrush, which generated unidirectional bottom currents, because in large tsunamis, the ratio of wave height to water depth was high due to the relative shallowness of the basin; (2) off-surge (backwash) from coastal and shallow offshore areas, which generated sand-laden underflows as jets; and (3) wave action, which generated oscillatory and combined flows. Off-surge transported the sand from the coastal areas. Onrush over the muddy sea bottom may have suspended some muds, but after delivery of the sand, onrush from a subsequent tsunami would have scoured and reworked it. Small tsunamis would have generated wave action. Bed thickness, as an indicator of the volume of sediment transported, is likely related to the amount of run-up and consequent backwash. The variation in current direction probably reflects shoreline configuration and sand distribution, interference, and location of the faults that were the source of the tsunamis. The symmetrical ripples were likely formed by post-tsunami oscillations (seiches) in the partially enclosed basin, although some of the smaller bed forms may be from storm reworking as well. Stacked and amalgamated sandstone beds probably reflect multiple tsunami events over a relatively short span of time. The rapid westward disappearance of sandstone (quartzite) is explained as resulting from the increased distance from the nearshore sand source. The northward and southward decrease may be for the same reason, or geomorphological differences along the eastern margin of the basin. Tsunamis would have affected other parts of the basin, but none has been specifically identified.

Deformation

The absence of oriented fold axes and lack of other evidence for a consistent paleoslope at the local or regional scale indicate that local, gentle crinkling and folding of mudstone laminae and sandstone beds were caused by in situ deformation after deposition and not by hydrodynamic processes or sediment density contrast involved in sedimentation. Earthquake shock explains these features. The small pits may be due to dewatering or gas escape triggered by shaking.

Common seismic activity explains the disruption, cracking, brecciation, and sediment injection features in the mudstone, as well as the cracks and dike arrays associated with the sandstones, because it caused ubiquitously directed compressional, extensional, and shear stresses, liquefaction, dewatering, and sediment mobilization. The injection direction was upward in mudstones, whereas dikes emanating from sandstone beds show both downward and upward injection. Interconnected patterns of dikes and cracks on bedding planes suggest there was a relatively narrow range of lateral distance permitted before the mud failed and injection took place. The quasi-linear orientation of some examples may be perpendicular to the direction of the epicenter and might reflect inhomogeneities imparted by the P-wave. Lenticular bedding in sandstones also influenced the orientation of small dikes, as did ripples, which partially confined the sinusoidal dikes belonging to the *Manchuriophycus* form to troughs that contained thicker mud. The absence of unequivocal

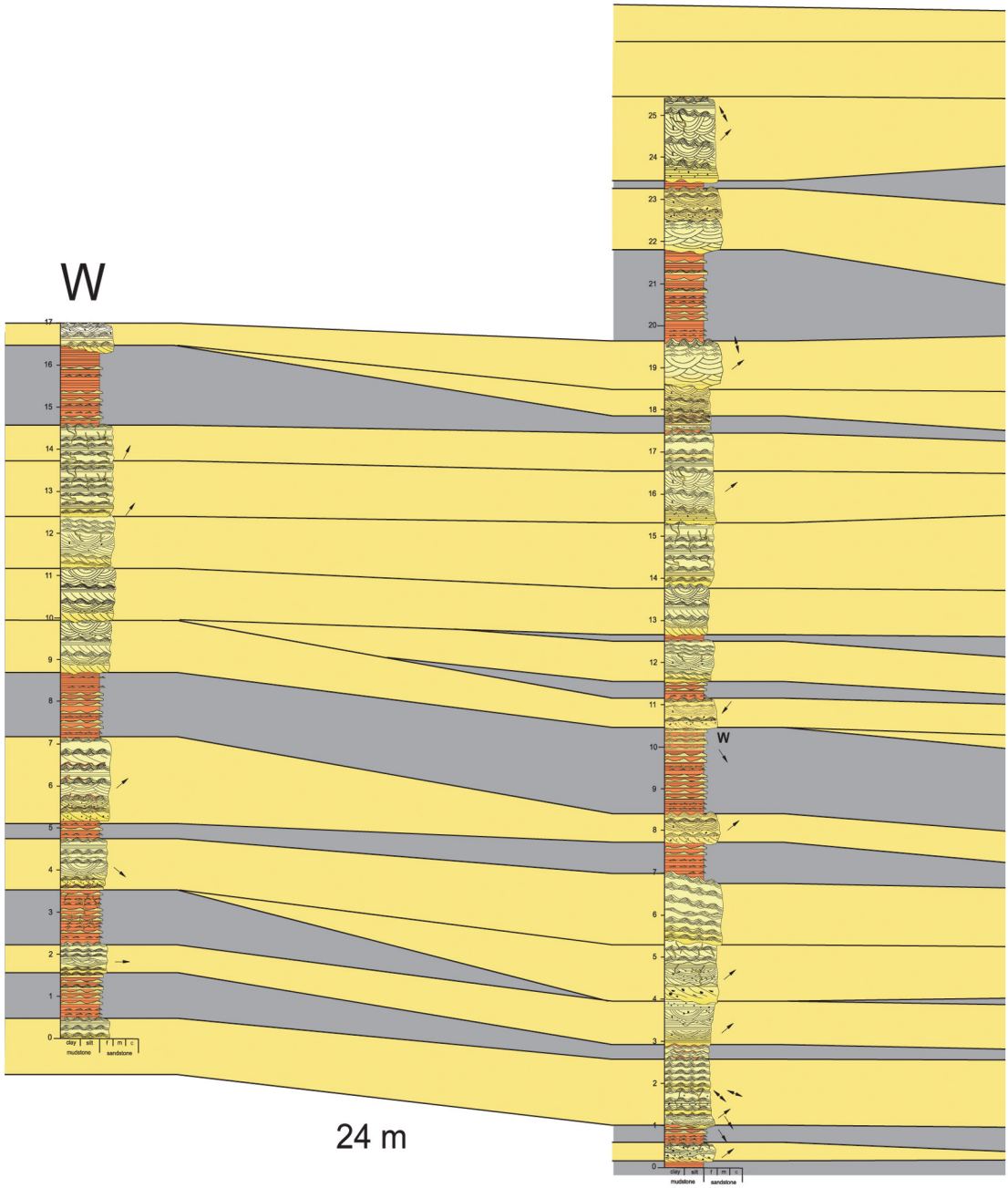

Figure 17. Closely spaced sections measured in the road cuts and on the hillside in the vicinity of Sunrift Gorge, Glacier National Park (48°40.708′N, 113°35.745′W), covering an interval just above the base of the formation. See Figure 4 for legend and abbreviations.

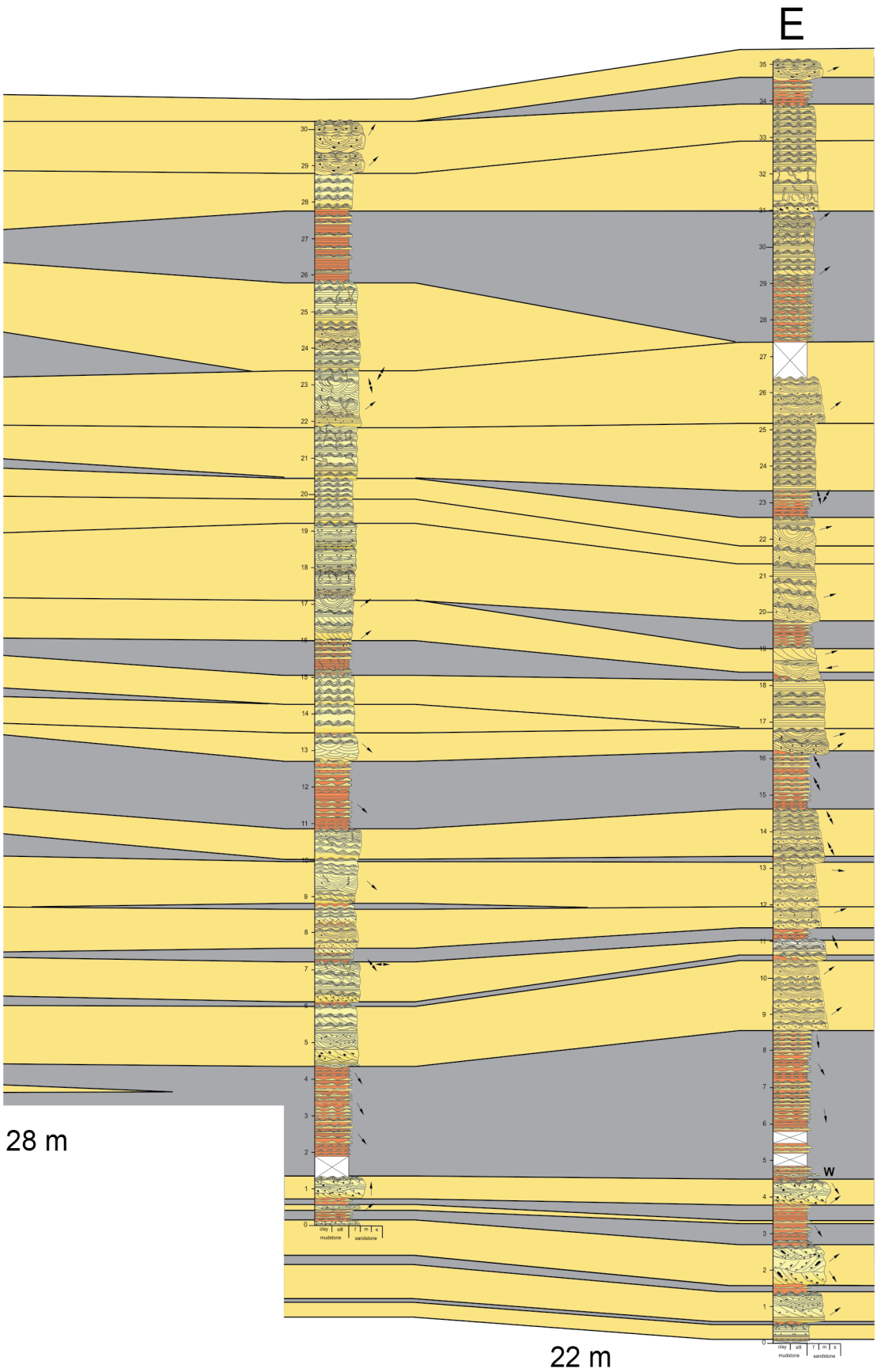

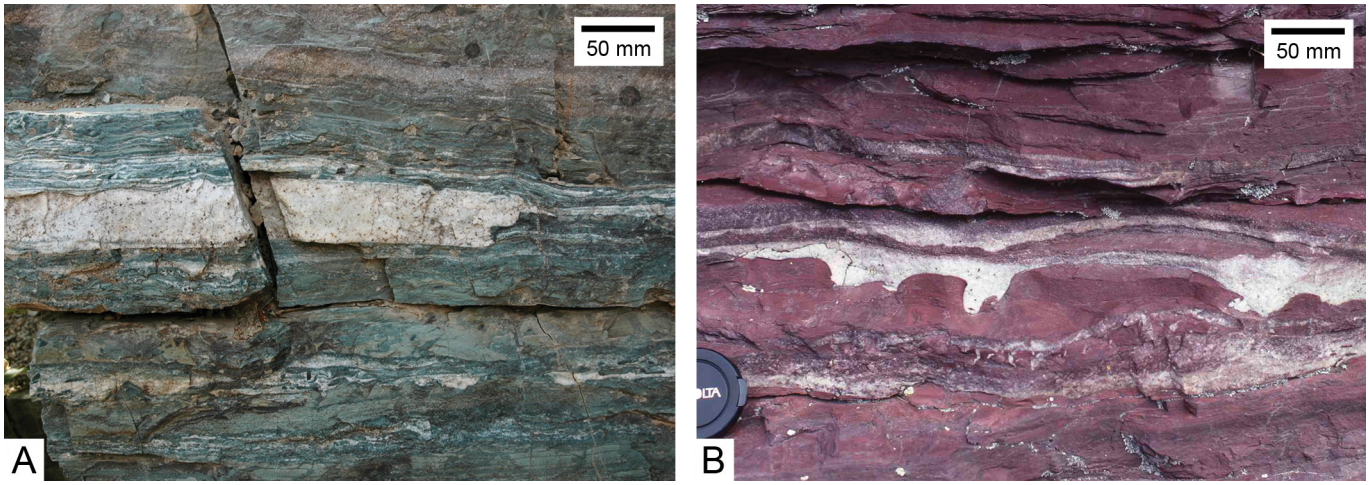

Figure 18. Scoured bases of thin sandstone beds. Sunrift Gorge. (A) Broad shallow gutter. (B) Gutter-like grooves.

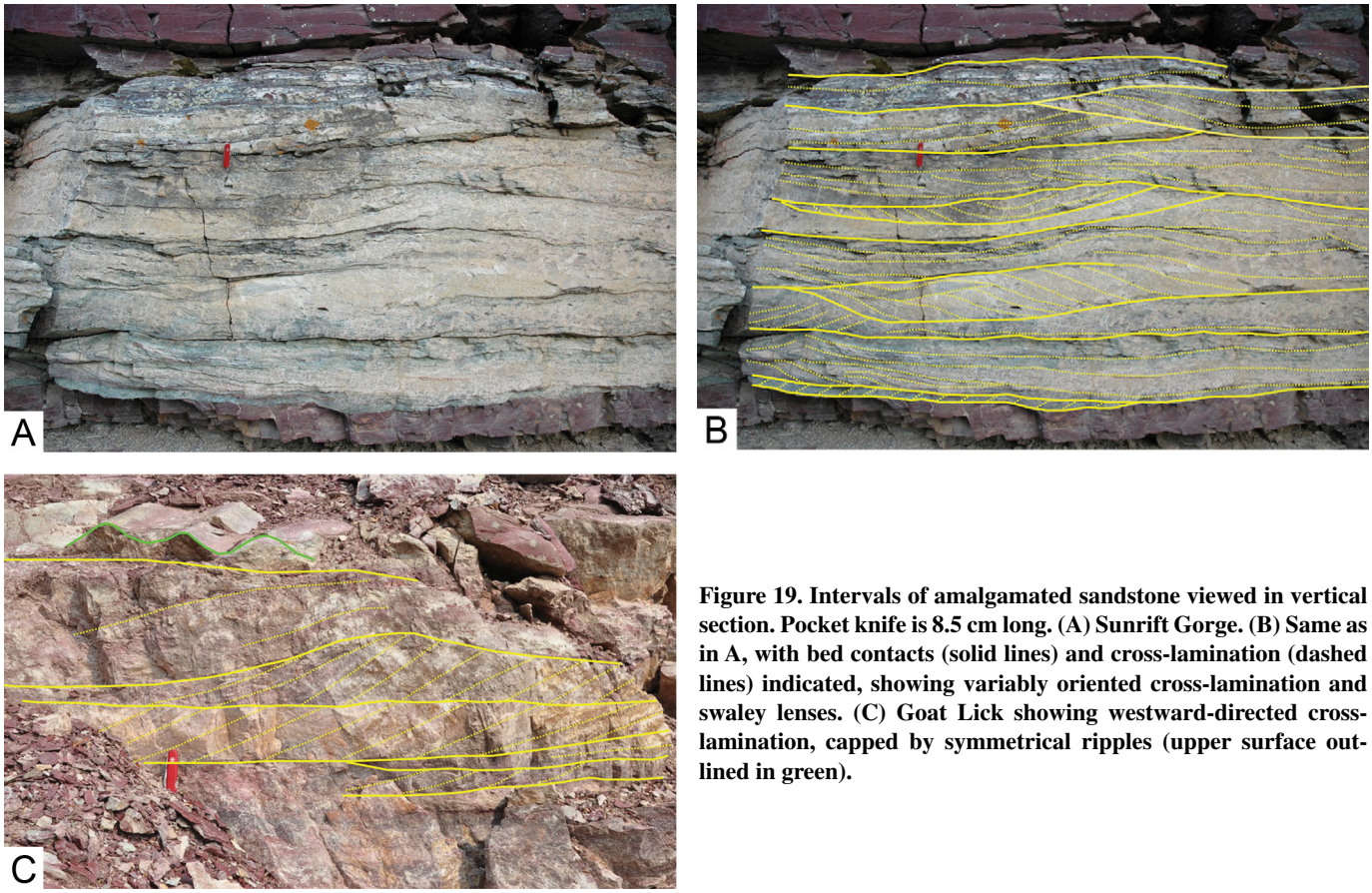

Figure 19. Intervals of amalgamated sandstone viewed in vertical section. Pocket knife is 8.5 cm long. (A) Sunrift Gorge. (B) Same as in A, with bed contacts (solid lines) and cross-lamination (dashed lines) indicated, showing variably oriented cross-lamination and swaley lenses. (C) Goat Lick showing westward-directed cross-lamination, capped by symmetrical ripples (upper surface outlined in green).

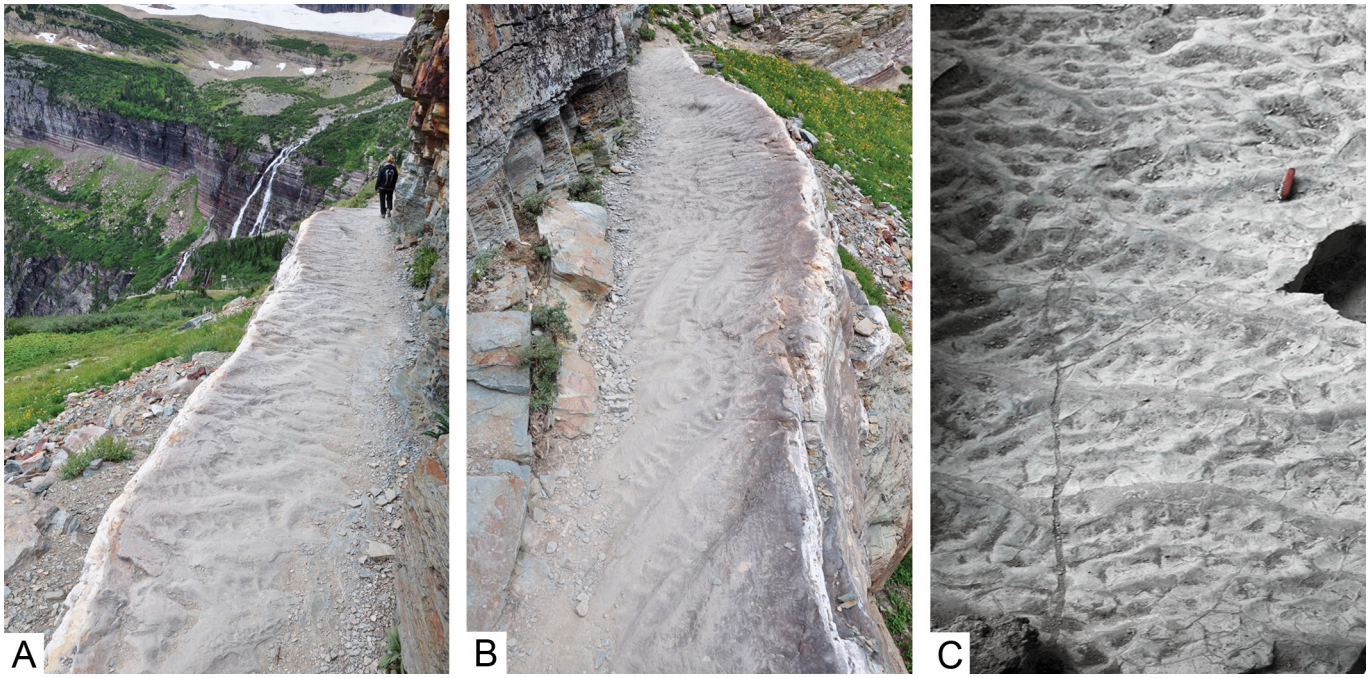

Figure 20. Bedding surfaces of sandstone. (A) View westward along Grinnell Glacier trail showing variably oriented and undulating large symmetrical ripple crests with subordinate smaller symmetrical ripples in the troughs at right angles. Person at far end. (B) Same bedding plane viewed eastward from the western end showing undulating large symmetrical ripple crests and smaller ones in the troughs ("ladder-backed" ripples). (C) Larger symmetrical ripples with smaller straight-crested and interference ripples in the troughs. Sunrift Gorge.

desiccation cracks filled by sediment derived from above rules out the possibility that some crack arrays could have overprinted preexisting cracks from subaerial exposure.

The fairly minor vertical distortion of cracks and common brecciation of the mudstone are further evidence for a relatively low water content of the clayey sediment, although this was enough to allow some dewatering and shrinkage when subjected to shaking. The length of folded sand-filled cracks projecting downward from sandstone shows a water content of up to ~50%, but typically less.

DISCUSSION

The Grinnell Formation has been universally interpreted to record deposition on alluvial floodplains, playas, or tidal flats (e.g., Price, 1964; Collins and Smith, 1977; McMechan, 1981; Horodyski, 1983; Koopman and Binda, 1985; Höy, 1992; Winston, 1986a, 1986c, 1989b, 1990, 2016; Winston and Link, 1993; Chandler, 2000; Slotznick et al., 2016). These interpretations were based primarily on the ubiquitous "mudcracks," which were assumed to be due to desiccation during subaerial exposure. In detail, however, these crack arrays lack the fundamental characteristics of subaerial exposure, such as a V-shape cross section with gravitational infilling from above, even though in many examples, a superficially similar polygonal pattern is present. Instead, deformation was clearly intrastratal, having formed under very shallow burial conditions (Pratt, 1998a). Other examples of crack arrays filled with upward-injected material, as well as small sandstone dikes exhibiting either or both upward and downward injection into enclosing muds, have also been interpreted as seismites, caused by earthquake shaking (e.g., Pratt, 1998a; Törő and Pratt, 2015a, 2015b, 2016; Leitner et al., 2017). There is no other obvious mechanism to simultaneously dewater muddy sediment and liquefy and mobilize silt and sand, as well as, in many cases, cause folding of the crack fills and brecciation of the matrix during the same or a subsequent event. Syneresis of clays (Burst, 1965) or bottom covering by microbial mats (Harazim et al., 2013) are passive phenomena that do not generate cyclic shear stresses. Wave impact (Winston and Smith, 2016) cannot account for substratal shrinkage and injection below the seafloor that shows no evidence of major scouring and reworking. The small-scale folding of some thin intervals was also due to synsedimentary earthquakes, as it indicates intermittent compressive stresses in a low-energy setting with no appreciable slope. Because deformation would affect both facies together, it is not due to gravitational effects from a density contrast due to passive loading of one sediment type on another (Owen, 2003). Other units in the Belt Supergroup exhibit a range of deformation features, some similar and some different—a function of sediment composition and rheology (Pratt, 1994, 1998a, 1998b, 2001, 2017). These kinds of features are present in many other sedimentary units, but their significance as a signal of syndepositional tectonic activity may have been overlooked (Pratt, 2018). Mudcracks are not always undisputed evidence for subaerial exposure.

The muds were not "soupy"; they were initially cohesive, and then they became stiff and subject to brittle failure at or near the sediment-water interface. This degree of consolidation before burial is a phenomenon that is unlikely to occur passively on the seafloor. Cyclic loading of saturated clays under undrained conditions, such as from earthquakes, can lead to failure because of the increase in pore pressure and loss of shear strength. If clays are allowed

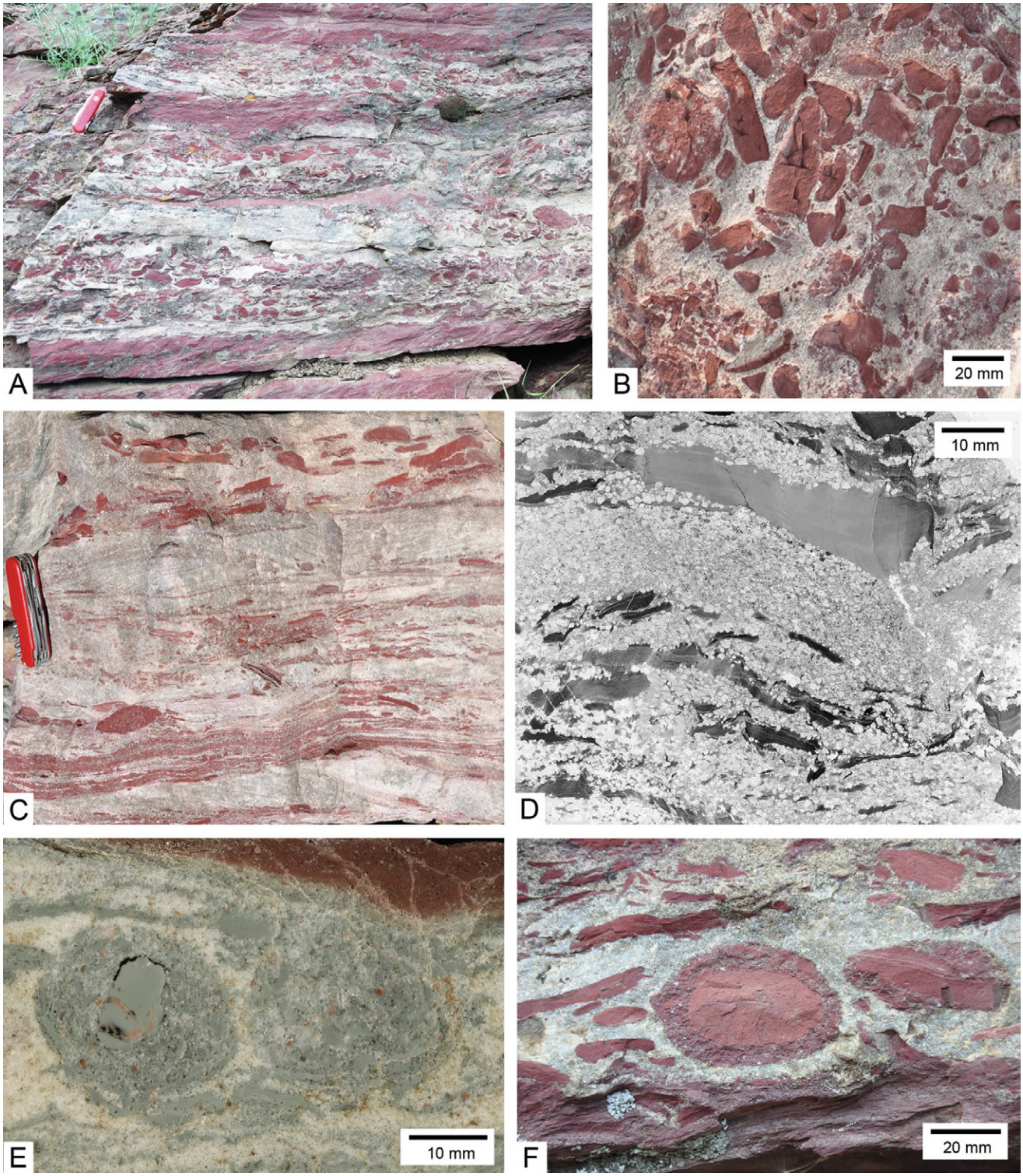

Figure 21. Mudstone intraclasts in sandstone. (A) Road cut west of Sunrift Gorge showing stacked cross-laminated sandstone thin beds with abundant angular to rounded intraclasts. (B) Bedding surface showing angular intraclasts of varying size and shape. Scale in centimeters. (C) Plane- and cross-laminated sandstone with angular intraclasts ranging from coarse sand to pebble sized. Cross-lamination shows unidirectional flow to both the right and left. Pocket knife is 8.5 cm in length. (D) Optical scan of thin section showing well-sorted, medium- to coarse-grained quartz sand and angular intraclasts of varying size. Intraclasts are variably squeezed and penetrated by sand grains. (E) Two "mudballs" composed of agglomerated quartz sand and subangular to rounded intraclasts. Large intraclast in core of left "mudball" contains sand-filled cracks. (F) Angular to rounded intraclasts with the two large rounded ones coated in quartz sand and mud forming "armored mudballs."

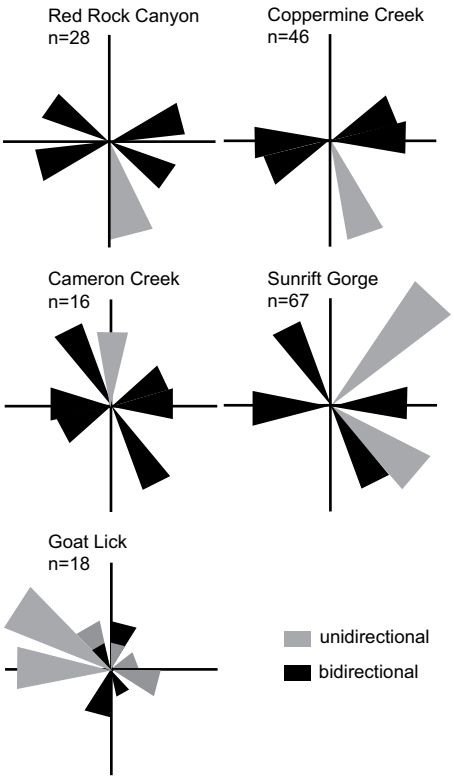

Figure 22. Rose diagrams showing paleocurrent directions indicated by unidirectional cross-lamination from asymmetrical ripples and crests of symmetrical ripples on bed surfaces, measured at the five measured sections.

to drain, settlement occurs, the water content decreases, and the shear strength increases (e.g., Nieto Leal and Kaliakin, 2013; Andersen, 2015). Thus, episodic shaking due to low-magnitude earthquakes may have contributed to syndepositional stiffening of argillaceous sediment in the Grinnell Formation. This has been suggested in passing as a mechanism for causing intervals of anomalous overconsolidation in muddy successions (Pratt, 1998b), but it needs to be explored further.

Figure 25 summarizes the inferred depositional setting of the Belt Basin during Ravalli Group time. Silt and clay were deposited from low-density turbidity currents and hemipelagic fallout from hypopycnal plumes (e.g., Schieber, 2016). These originated from fluvial discharge far to the west, likely as flooding events rather than sustained hyperpycnal flows (e.g., Zavala et al., 2006, 2011; Wilson and Schieber, 2017). Occasional gentle reworking by storms (or weak tsunamis) took place, but evidence for deposition by storm-generated sediment gravity flows, such as ripples recording combined flow (e.g., Plint, 2014), does not appear to be present. Indeed, the Belt Basin seems not to have been a particularly stormy sea (Pratt, 2001), and formation of stromatolites within the photic zone is further evidence for a shallow storm wave base for the Grinnell Formation as a whole. This is not unexpected if the basin was located at or near the equator.

Halite crystal casts and molds represent displacive growth in and on the upper layer of mud, but the crystals dissolved when the overlying water freshened. Rather than representing in situ evaporation and corroborating a playa setting, the halite records occasional development of density stratification due to sluggish circulation and bottom-hugging hypersaline brines that were concentrated elsewhere, presumably in shallow nearshore areas, probably broadly to the east. The apparent absence of halite in the correlative Burke, Revett, and St. Regis Formations to the west could indicate shallower water, above the pycnocline, or there was westward dissipation of the brines closer to the sources of riverine input. Similar zoned halite crystal casts and molds in both siliciclastic and carbonate mudstones associated with crack arrays and other synsedimentary deformation features occur in many other units (e.g., Spencer and Demicco, 1993; Eriksson et al., 2005; Paik and Kim, 2006; Martill et al., 2007; Rychliński et al., 2014). The bathymetric interpretation of some of these merits reconsideration.

In the most often expressed environmental interpretation of the Grinnell Formation, sandstone beds have been regarded as fluvial sand sheets from flooding events. The absence of channel-form features and trough cross-bedding was explained by the interpretation that both they and the mudstone are sheetflood deposits with planar geometries (Winston, 1986a, 1986c, 1989b, 1990, 2016; Winston and Link, 1993). Setting aside the difficulty in reconciling this scenario with the muds of a floodplain being sourced from the west and intercalated fluvial sands coming from the northeast, flashy discharge leading to unconfined flow is usually associated geographically with nearby alluvial fans and slopes or channels as overbank or avulsion flooding phenomena (e.g., Fisher et al., 2007), but no evidence for channels is present anywhere in the Grinnell Formation or apparently in the correlative units to the west (Winston, 2016). Ephemeral sheetflood deposits are commonly transitional to upper-flow-regime beds characterized by low-angle to sinusoidal cross-bedding and abundant plane-lamination (e.g., Hampton and Horton, 2007; Lowe and Arnott, 2016), although there is much variability, and many examples reflect lower-energy flows (North and Davidson, 2012). The upper surface of sheetflood deposits may be reworked by eolian processes. In the Grinnell Formation, however, most sandstones exhibit lower-flow-regime, unidirectional cross-lamination with variable and commonly opposing current directions, two sizes of oscillation ripples, and in some instances combined-flow structures. These are incompatible with a fluvial origin, either on a subaerially exposed mud flat or shallow playa. Furthermore, the generally rounded nature of the sand grains is more simply explained as indicating a shallow-marine rather than fluvial source, which would typically supply texturally immature sediment, in contrast to the reworking that occurs under protracted wave action. In addition, first-cycle eolian sands tend to remain angular to subangular, except perhaps in situations where there is considerable back-and-forth motion over long time periods (Folk, 1978).

The sandstones are interpreted here as tsunamites (or tsunamiites), but the combination of processes envisaged for sediment transport, deposition, and reworking in a tectonically highly active, shallow, flat-bottomed, nearly enclosed sea like the Belt Basin has no known modern analogs, and tsunami effects are not well understood in present-day offshore settings in general (Dawson and Stewart, 2008). Reversing flows are created by onrush in shallow bays ,which also experience oscillation long after the tsunami waves have impacted the coast (Lacy et al., 2012). Backwash, or off-surge, transports sediment offshore, but the sedimentary architecture in Holocene deposits is essentially unknown (e.g., Noda et al., 2007; Toyofuku et al., 2014). The first requirement is that they have to be emplaced beyond the depth of reworking by storm waves (Weiss and Bahlburg, 2006). The second, for Phanerozoic examples, is that they have to have escaped complete bioturbation.

Putative ancient tsunamites in offshore settings are variable, although few have been recognized. In the Miocene of eastern Italy, three examples from a deep-water mudstone succession containing thin turbidites share some similarities with those in the Grinnell Formation. They consist of sets of stacked, thin, cross-laminated, graded sandstone beds with erosive bases (Smit et al., 2012). Variably directed cross-lamination and climbing ripple cross-lamination are present in the lower set, whereas trough cross-lamination is present in the middle one, and the upper one has a channelized base and contains a layer with wave ripple cross-lamination. Sandstones in the Grinnell Formation differ in lacking trough cross-lamination. Features ascribed to tsunamis in limestones of the Helena Formation above the Grinnell Formation

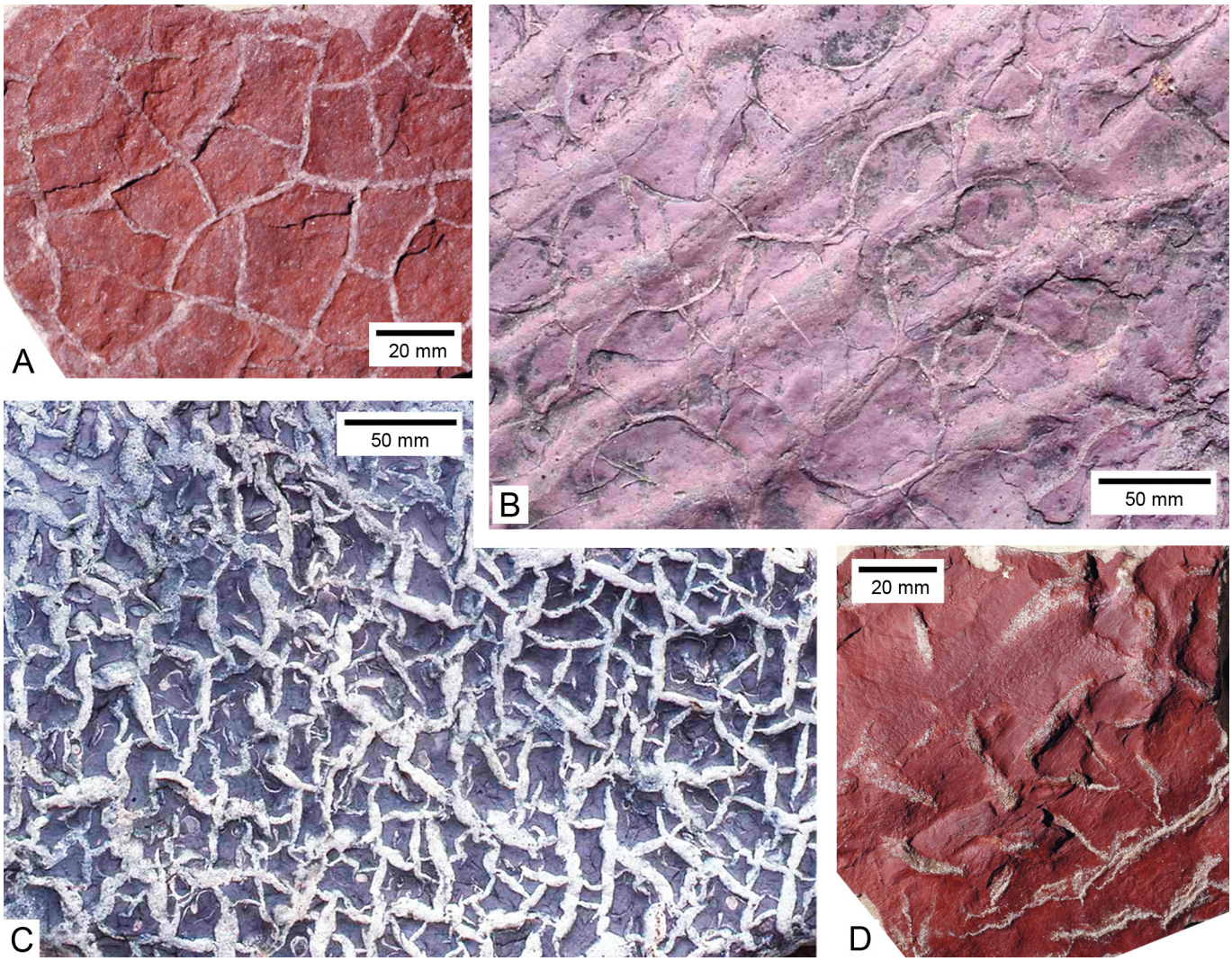

Figure 23. Bedding plane surfaces of sand-filled dikes (cracks) projecting from sandstone into mudstone. (A) Underside of bed with dense network of curving spindle-shaped and parallel-sided dikes of two different size groups. (B) Upper surface with network of straight to gently curving, parallel-sided dikes on top surface. (C) Upper surface with isolated lenticular dikes above crest of large ripple and irregularly linear dikes in trough. A sparse network of dikes is present on the bottom bedding surface. (D) Upper surface of network of parallel-sided sinusoidal (in symmetrical ripple troughs) and straight cracks (crossing ripple crests). (A tracing of this surface is fig. 1C of Pratt, 1998a.)

are understandably different, and they include: (1) intraclastic rudstone as flat-pebble conglomerate; (2) deep scour surfaces and gutters filled with fragments of molar-tooth structure; and (3) sandy ooid grainstone, locally with hummocky cross-stratification. These punctuate the argillaceous lime mudstone succession and are therefore anomalous in terms of background processes (Pratt, 1998b, 2001).

Upper Cambrian mixed carbonate-siliciclastic facies in north-central Montana similarly possess evidence of scour and wave action of a much greater magnitude than what is indicated by background processes, which generated lenses of flat-pebble conglomerate that punctuate the succession (Pratt, 2002). In the middle Cambrian of western Argentina, the host facies is bioturbated lime mudstone, and the intraclasts are fragments of cemented burrow margins, but otherwise wave-induced features appear to be absent (Pratt and Bordonaro, 2007). In both these cases, there is no allochthonous sediment, which may be due to basin shape and too great a distance from coastal areas. Examples of hummocky cross-stratification and imbricated intraclasts at the limit or below ambient storm wave base may be due to later stages of the tsunami wave train, post-tsunami seiching, or reworking by subsequent tsunamis; oscillation ripples may have the same origins, in addition to storm action.

It is premature to devise a facies model for tsunamites in deeper-water settings, especially given the wide range of basin types. In addition to the search for modern examples, reevaluation of beds hitherto interpreted as tempestites in some ancient successions should turn up candidates that may plausibly be considered tsunami-generated.

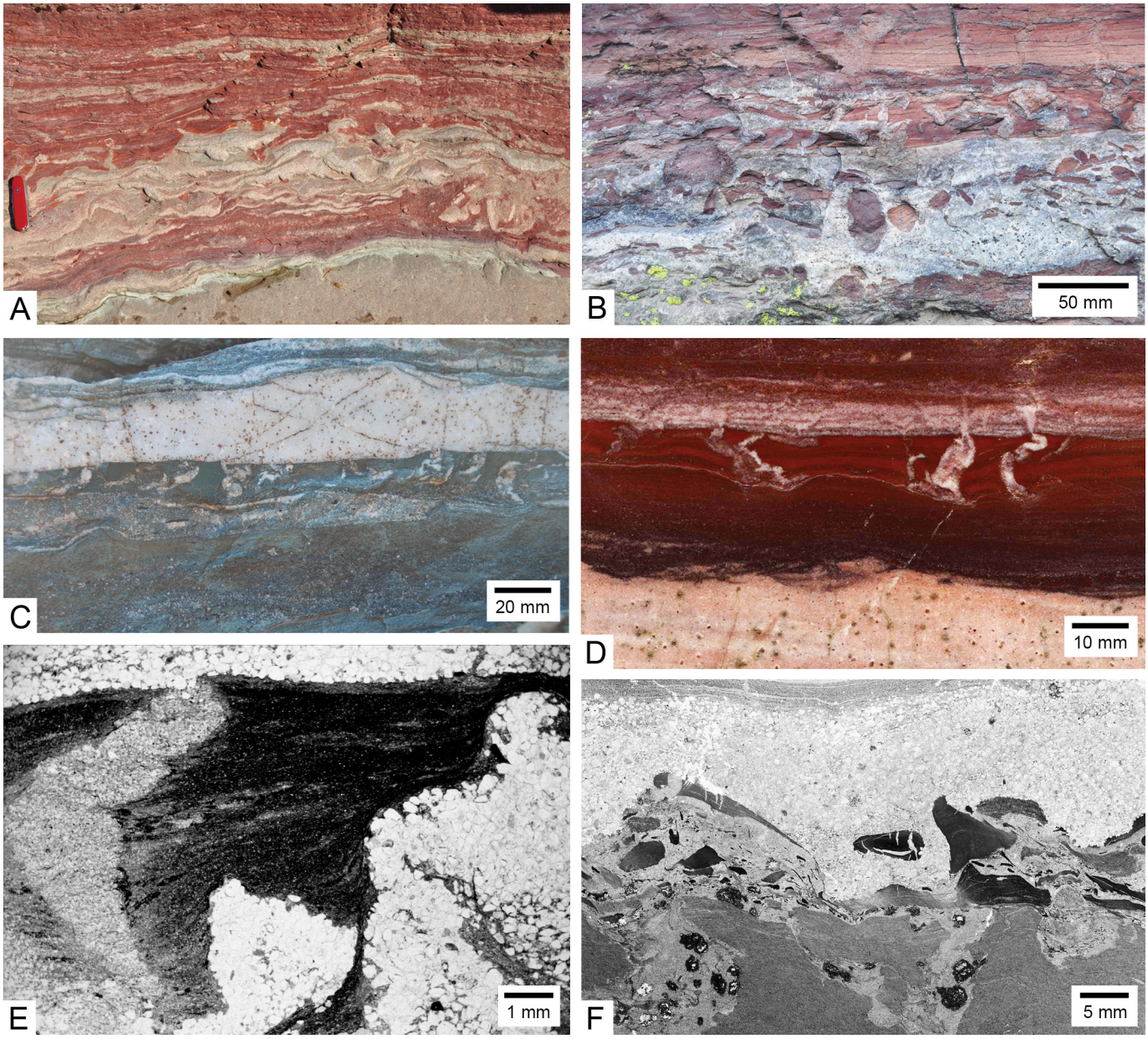

Figure 24. Views perpendicular to bedding of sediment-filled cracks (dikes) in mudstone associated with sandstone. (A) Outcrop showing folded dikes projecting downward (and upward, at right side) from bottom of a thin bed of cross-laminated sandstone into laminated mudstone and sandstone. (B) Outcrop of sand-filled dikes and sills projecting above intraclast-rich sandstone thin bed. (C) Outcrop of folded sand-filled dikes projecting downward from rippled sandstone thin bed. (D) Polished surface of folded dikes projecting downward from plane-laminated sandstone into laminated mudstone (argillite, shale). The cross-laminated sandstone bed a few centimeters below is undeformed. (E) Thin section photomicrograph of folded sand-filled dikes (lower center and right) projecting downward from sandstone bed (top), adjacent to silt-filled dike (left) that was sourced from a layer that was scoured off when the sandstone was deposited (also Pratt, 2017, fig. 7D). (F) Optical scan of thin section showing two dikes filled with clay, silt, and mudstone intraclasts penetrating upward through claystone into base of thin sandstone bed.

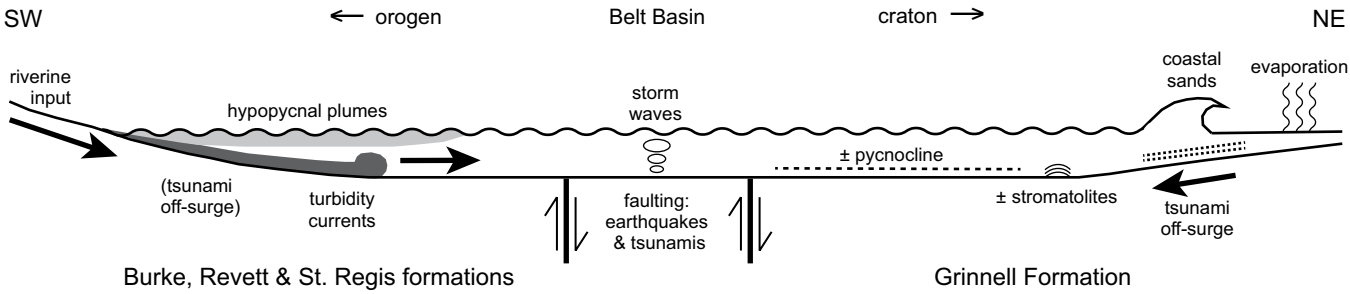

Figure 25. Hypothetical southwest-northeast cross section of the shallow Belt Basin during deposition of the Ravalli Group. Texturally and compositionally immature sediment entered the basin from the eroding orogen to the west and was distributed by turbidity currents and hypopycnal plumes, with only mud reaching distal areas. Occasional weak storms reworked the sea bottom. A pycnocline occasionally developed in the northeastern region from the influx of brines from adjacent shallow areas; stromatolites accreted at several times. Faults generated frequent earthquakes ranging from tremors to strong events that caused liquefaction, as well as common tsunamis of various sizes. Tsunami off-surge transported texturally and compositionally mature sand from coastal areas in the northeast. Off-surge likely affected the western side of the basin as well, but specific features have not yet been identified.

CONCLUSIONS

Misunderstood for more than a century, the Mesoproterozoic Grinnell Formation of western North America is revealed here to have been deposited not on floodplains, playas, or tidal flats. Rather, the mudstone (argillite) consists of sediment derived from the west, and it represents distal turbidites and hemipelagic fallout from hypopycnal plumes in a shallow basin subject to reworking by no more than gentle wave action during weak storms. Several stromatolite-bearing horizons indicate deposition within the photic zone. Bedding planes with halite crystal casts and molds are not evidence of in situ subaerial exposure; instead, they represent the influx of bottom-hugging brines that had evaporated in coastal regions probably to the east. Deposited layers of chlorite and illite were not flocculent, but instead clay laminae acquired a degree of stiffness that left them prone to brittle failure on the seafloor. Frequent strong earthquake shock caused a combination of shrinkage and rupturing of the muddy layers and concomitant upward injection of clay, silt, and clay intraclasts into crack arrays of various shapes on bedding planes. These cracks arrays are not desiccation features, despite their superficial similarity to subaerial mudcracks.

Tabular to lenticular sandstone (quartzite) beds punctuating the mudstone succession are cross-laminated from variably unidirectional and oscillatory currents but lack evidence of channeling. The striking contrast between the coarser, rounded sand and the angular silt in the mudstone points to a coastal source to the east, where the sand was winnowed and rounded by protracted wave action. This sand was delivered by the backwash from tsunamis that repeatedly swept across the shallow basin; mud intraclasts eroded from the sea bottom were incorporated. The sands were often reworked by later tsunamis, seiching, and backwash, as well as perhaps subsequent onrush. Sandstones were likewise affected by earthquake shock, and the tops and bottoms of beds commonly show sand-filled dikes recording both upward and downward injection into concomitantly formed shrinkage cracks in mud.

The Grinnell Formation joins other units in the Belt Supergroup, be they siliciclastic or carbonate, in exhibiting a striking array of sedimentary features. These not only have fundamental implications for bathymetry, deposition, salinity, paleoclimate, and paleoceanography, but they also demonstrate that the Belt Basin was tremendously active tectonically, which gave rise not only to the extraordinary rate of subsidence, but also to repeated earthquakes and tsunamis. When the deposits of other epeiric seas and shelf margins are parsed for comparable phenomena, hitherto overlooked or underappreciated counterparts will likely be found.

ACKNOWLEDGMENTS

Fieldwork was funded by the Natural Sciences and Engineering Research Council (NSERC) of Canada through Research and Discovery grants awarded to Pratt. The Consejo Nacional de Investigaciones Científicas y Técnicas (CONICET) of Argentina provided financial support for Ponce. We thank E.C. Turner and R.G. Brown for help in the field in the early 1990s and E. Wiens and S. Dasgupta in 2013, and the staff of both national parks for issuing research permits. We are grateful to D. Winston and D.G.F. Long for discussion and debate over the years, and L.B. Aspler and an anonymous reviewer for refereeing the manuscript.

REFERENCES CITED

Allen, P.A., 1981, Wave-generated structures in the Devonian lacustrine sediments of south-east Shetland and ancient wave conditions: Sedimentology, v. 28, p. 369–379, https://doi.org/10.1111/j.1365-3091.1981.tb01686.x.

Andersen, K.H., 2015, Cyclic soil parameters for offshore foundation design, *in* Meyer, V., ed., Frontiers in Offshore Geotechnics III: London, Taylor & Francis, p. 5–82, https://doi.org/10.1201/b18442-4.

Aspler, L.B., Chiarenzelli, J.R., and Bursey, T.L., 1994, Ripple marks in quartz arenites of the Hurwitz Group, Northwest Territories, Canada: Evidence for sedimentation in a vast, Early Proterozoic, shallow, freshwater lake: Journal of Sedimentary Research, v. A64, p. 282–298.

Burst, J.F., 1965, Subaqueously formed shrinkage cracks in clay: Journal of Sedimentary Petrology, v. 35, p. 348–353, https://doi.org/10.1306/74D71271-2B21-11D7-8648000102C1865D.

Chandler, F.W., 2000, The Belt-Purcell Basin as a low-latitude passive rift: Implications for the geological environment of Sullivan type deposits, *in* Lydon, J.W., Höy, T., Slack, J.F., and Knapp, M.E., eds., The Geological Environment of the Sullivan Deposit, British Columbia: Geological Association of Canada, Mineral Deposits Division Special Publication 1, p. 82–112.

Clifton, H.E., and Dingler, J.R., 1984, Wave-formed structures and paleoenvironmental reconstruction: Marine Geology, v. 60, p. 165–198, https://doi.org/10.1016/0025-3227(84)90149-X.

Collins, J.A., and Smith, L., 1977, Genesis of cupriferous quartz arenite cycles in the Grinnell Formation (Spokane equivalent), Middle Proterozoic (Helikian) Belt-Purcell Supergroup, eastern Rocky Mountains, Canada: Bulletin of Canadian Petroleum Geology, v. 25, p. 713–735.

Cressman, E.R., 1989, Reconnaissance Stratigraphy of the Prichard Formation (Middle Proterozoic) and the Early Development of the Belt Basin, Washington, Idaho, and Montana: U.S. Geological Survey Professional Paper 1490, 80 p.

Dawson, A.G., and Stewart, I., 2008, Offshore tractive current deposition: The forgotten tsunami sedimentation process, *in* Shiki, T., Tsuji, Y., Yamazaki, T., and Minoura, K., eds., Tsunamiites: Features and Implications: Amsterdam, Netherlands, Elsevier, p. 153–161, https://doi.org/10.1016/B978-0-444-51552-0.00010-2.

Duke, E., and Lewis, R.S., 2010, Near infrared spectra of white mica in the Belt Supergroup and implications for metamorphism: The American Mineralogist, v. 95, p. 908–920, https://doi.org/10.2138/am.2010.3281.

Earhart, R.L., Mudge, M.R., and Connor, J.J., 1984, Belt Supergroup lithofacies in the Northern Disturbed Belt, northwest Montana, *in* McBane, J.D., and Garrison, P.B., eds., Northwest Montana and Adjacent Canada: Billings, Montana, Montana Geological Society, 1984 Field Conference and Symposium Guidebook, p. 51–66.

Eriksson, K.A., Simpson, E.L., Master, S., and Henry, G., 2005, Archaean (*c.* 2.58 Ga) halite casts: Implications for palaeoceanic chemistry: Journal of the Geological Society [London], v. 162, p. 789–799, https://doi.org/10.1144/0016-764904-120.

Eslinger, E.V., and Savin, S.M., 1973, Oxygen isotope geothermometry of the burial metamorphic rocks of the Precambrian Belt Supergroup, Glacier National Park: Geological Society of America Bulletin, v. 84, p. 2549–2560, https://doi.org/10.1130/0016-7606(1973)84<2549:OIGOTB>2.0.CO;2.

Eslinger, E.V., and Sellars, B., 1981, Evidence for the formation of illite from smectite during burial metamorphism in the Belt Supergroup, Clark Fork, Idaho: Journal of Sedimentary Petrology, v. 51, p. 203–216.

Fenton, C.L., and Fenton, M.A., 1937, Belt Series of the north: Stratigraphy, sedimentation, paleontology: Geological Society of America Bulletin, v. 48, p. 1873–1969, https://doi.org/10.1130/GSAB-48-1873.

Fisher, J.A., Nichols, G.J., and Waltham, D.A., 2007, Unconfined flow deposits in distal sectors of fluvial distributary systems: Examples from the Miocene Luna and Huesca systems, northern Spain: Sedimentary Geology, v. 195, p. 55–73, https://doi.org/10.1016/j.sedgeo.2006.07.005.

Folk, R.L., 1978, Angularity and silica coatings of Simpson Desert sand grains, Northern Territory, Australia: Journal of Sedimentary Petrology, v. 48, p. 611–624.

Gardner, D.W., 2008, Sedimentology, Stratigraphy, and Provenance of the Upper Purcell Supergroup, Southern British Columbia: Implications for Syn-Depositional Tectonism, Basin Models, and Paleogeographic Reconstructions [M.S. thesis]: Victoria, British Columbia, Canada, University of Victoria, 76 p.

Hampton, B.A., and Horton, B.K., 2007, Sheetflow fluvial processes in a rapidly subsiding basin, Altiplano plateau, Bolivia: Sedimentology, v. 54, p. 1121–1147, https://doi.org/10.1111/j.1365-3091.2007.00875.x.

Harazim, D., Callow, R.T., and McIlroy, D., 2013, Microbial mats implicated in the generation of intrastratal shrinkage ('synaeresis') cracks: Sedimentology, v. 60, p. 1621–1638, https://doi.org/10.1111/sed.12044.

Harrison, J.E., Whipple, J.W., and Kidder, D.L., 1993, Belt Supergroup stratigraphy and structure, north-central Belt Basin, northwestern Montana, *in* Link, P.K., ed., Geologic Guidebook to the Belt-Purcell Supergroup, Glacier National Park and Vicinity, Montana and Adjacent Canada: Pocatello, Idaho, Belt Association, p. 1–19.

Harrison, J.E., Whipple, J.W., and Lidke, D.J., 1996, Geologic Map of the Western Part of the Cut Bank 1° × 2° Quadrangle, Northwestern Montana: U.S. Geological SurveyMiscellaneous Investigations Series Map I-2593, scale 1:250,000.

Hein, F.J., and McMechan, M.E., 1994, Proterozoic and Lower Cambrian strata of the Western Canada sedimentary basin, *in* Mossop, G.D., and Shetsen, I., compilers, Atlas of the Western Canada Sedimentary Basin: Calgary/Edmonton, Alberta, Canadian Society of Petroleum Geology and Alberta Research Council, p. 57–67.

Hill, R., and Mountjoy, E.W., 1984, Stratigraphy and sedimentology of the Waterton Formation, Belt Purcell Supergroup, Waterton Lakes National Park, *in* McBane, J.D., and Garrison, P.B., eds., Northwest Montana and Adjacent Canada: Billings, Montana, Montana Geological Society, 1984 Field Conference and Symposium Guidebook, p. 91–100.

Horodyski, R.J., 1983, Sedimentary geology and stromatolites of the Middle Proterozoic Belt Supergroup, Glacier National Park, Montana: Precambrian Research, v. 20, p. 391–425, https://doi.org/10.1016/0301-9268(83)90083-9.

Höy, T., 1989, The age, chemistry, and tectonic setting of the Middle Proterozoic Moyie sills, Purcell Supergroup, southeastern British Columbia: Canadian Journal of Earth Sciences, v. 26, p. 2305–2317, https://doi.org/10.1139/e89-196.

Höy, T., 1992, Geology of the Purcell Supergroup in the Fernie West-Half Map Area, Southeastern British Columbia: British Columbia Mineral Resources Division Bulletin 84, 157 p.

Irwin, M.L., 1965, General theory of epeiric clear water sedimentation: American Association of Petroleum Geologists Bulletin, v. 49, p. 449–459.

Jin, J., Harper, D.A.T., Cocks, L.R.M., McCausland, P.J.A., Rasmussen, C.M.Ø., and Sheehan, P.M., 2013, Precisely locating the Ordovician equator in Laurentia: Geology, v. 41, p. 107–110, https://doi.org/10.1130/G33688.1.

Koopman, H.T., and Binda, P.L., 1985, Preliminary observations on stratiform copper occurrences in the basal Siyeh Formation of Proterozoic age, southern Alberta, *in* Current Research Part B: Geological Survey of Canada Paper 85-1B, p. 133–140.

Kuhn, J.A., 1987, The Stratigraphy and Sedimentology of the Middle Proterozoic Grinnell Formation, Glacier National Park and the Whitefish Range, NW Montana [M.S. thesis]: Missoula, Montana, University of Montana, 122 p.

Lacy, J.R., Rubin, D.M., and Buscombe, D., 2012, Currents, drag, and sediment transport induced by a tsunami: Journal of Geophysical Research, v. 117, C09028, https://doi.org/10.1029/2012JC007954.

Leitner, C., Wiesmaier, S., Köster, M.H., Gilg, A., Finger, F., and Neubauer, F., 2017, Alpine halite-mudstone-polyhalite tectonite: Sedimentology and early diagenesis of evaporites in an ancient rift setting (Haselgebirge Formation, eastern Alps): Geological Society of America Bulletin, v. 129, p. 1537–1553, https://doi.org/10.1130/B31747.1.

Link, P.K., Fanning, C.M., Lund, K.I., and Aleinikoff, J.N., 2007, Detrital-zircon populations and provenance of Mesoproterozoic strata of east-central Idaho, U.S.A.: Correlation with the Belt Supergroup of southwest Montana, *in* Link, P.K., and Lewis, R.S., eds., Proterozoic Geology of Western North America and Siberia: Society for Sedimentary Geology (SEPM) Special Publication 86, p. 101–128, https://doi.org/10.2110/pec.07.86.0101.

Link, P.K., Stewart, E.D., Steel, T., Sherwin, J., Hess, L.T., and McDonald, C., 2016, Detrital zircons in Mesoproterozoic upper Belt Supergroup in the Pioneer, Beaverhead, and Lemhi ranges, Montana and Idaho: The Big White Arc, *in* MacLean, J.S., and Sears, J.W., eds., Belt Basin: Window to Mesoproterozoic Earth: Geological Society of America Special Paper 522, p. 163–183, https://doi.org/10.1130/2016.2522(07).

Lowe, D.G., and Arnott, R.W.C., 2016, Composition and architecture of braided and sheetflood-dominated ephemeral fluvial strata in the Cambrian–Ordovician Potsdam Group: A case example of the morphodynamics of early Phanerozoic fluvial systems and climate change: Journal of Sedimentary Research, v. 86, p. 587–612, https://doi.org/10.2110/jsr.2016.39.

Lydon, J.W., 2000, A synopsis of the current understanding of the geological environment of the Sullivan deposit, *in* Lydon, J.W., Höy, T., Slack, J.F., and Knapp, M.E., eds., The Geological Environment of the Sullivan Deposit, British Columbia: Geological Association of Canada, Mineral Deposits Division Special Publication 1, p. 12–31.

Lydon, J.W., 2007, Geology and metallogeny of the Belt-Purcell Basin, *in* Goodfellow, W.D., ed., Mineral Deposits of Canada: A Synthesis of Major Deposit Types, District Metallogeny, the Evolution of Geological Provinces, and Exploration Methods: Geological Association of Canada, Mineral Deposits Division Special Publication 5, p. 581–607.

Martill, D.M., Loveridge, R., and Heimhofer, U., 2007, Halite pseudomorphs in the Crato Formation (Early Cretaceous, late Aptian–early Albian), Araripe Basin, northeast Brazil: Further evidence for hypersalinity: Cretaceous Research, v. 28, p. 613–620, https://doi.org/10.1016/j.cretres.2006.10.003.

McGimsey, R.G., 1985, The Purcell Lava, Glacier National Park, Montana: U.S. Geological Survey Open-File Report 85-0543, 191 p., https://doi.org/10.3133/ofr85543.

McMechan, M.E., 1981, The Middle Proterozoic Purcell Supergroup in the southwestern Rocky and southeastern Purcell Mountains, British Columbia, and the initiation of the Cordilleran miogeocline, southern Canada and adjacent United States: Bulletin of Canadian Petroleum Geology, v. 29, p. 583–621.

Nieto Leal, A., and Kaliakin, V.N., 2013, Behavior of Cohesive Soils Subjected to Cyclic Loading: An Extensive Review of Pertinent Literature: Newark, Delaware, Department of Civil and Environmental Engineering, University of Delaware, Research Report, 109 p.

Noda, A., Katayama, H., Sagayama, T., Suga, K., Uchida, Y., Satake, K., Abe, K., and Okamura, Y., 2007, Evaluation of tsunami impacts on shallow marine sediments: An example from the tsunami caused by the 2003 Tokachi-oki earthquake, northern Japan: Sedimentary Geology, v. 200, p. 314–327, https://doi.org/10.1016/j.sedgeo.2007.01.010.

North, C.P., and Davidson, S.K., 2012, Unconfined alluvial flow processes: Recognition and interpretation of their deposits, and the significance for palaeogeographic reconstruction: Earth-Science Reviews, v. 111, p. 199–223, https://doi.org/10.1016/j.earscirev.2011.11.008.

Owen, G., 2003, Load structures: Gravity-driven sediment mobilization in the shallow subsurface, *in* Van Rensbergen, P., Hillis, R.R, Maltman, A.J., and Morley, C.K., eds., Subsurface Sediment Mobilization: Geological Society, London, Special Publication 216, p. 21–34, https://doi.org/10.1144/GSL.SP.2003.216.01.03.

Paik, I.S., and Kim, H.J., 2006, Playa lake and sheetflood deposits of the Upper Cretaceous Jindong Formation, Korea: Occurrences and palaeoenvironments: Sedimentary Geology, v. 187, p. 83–103, https://doi.org/10.1016/j.sedgeo.2005.12.006.

Pehrsson, S.J., Eglington, B.M., Evans, D.A.D., Huston, D., and Reddy, S.M., 2016, Metallogeny and its link to orogenic style during the Nuna supercontinent cycle, *in* Li, Z.X., Evans, D.A.D., and Murphy, J.B., eds., Supercontinent Cycles Through Earth History: Geological Society, London, Special Publication 424, p. 83–94, https://doi.org/10.1144/SP424.5.

Pisarevsky, S.A., Elming, S.-Å., Pesonen, L.J., and Li, Z.-X., 2014, Mesoproterozoic paleogeography: Supercontinent and beyond: Precambrian Research, v. 244, p. 207–225, https://doi.org/10.1016/j.precamres.2013.05.014.

Plint, A.G., 2014, Mud dispersal across a Cretaceous prodelta: Storm-generated wave-enhanced sediment gravity flows inferred from mudstone microtexture and microfacies: Sedimentology, v. 61, p. 609–647, https://doi.org/10.1111/sed.12068.

Pratt, B.R., 1994, Seismites in the Mesoproterozoic Altyn Formation (Belt Supergroup), Montana: A test for tectonic control of peritidal carbonate cyclicity: Geology, v. 22, p. 1091–1094, https://doi.org/10.1130/0091-7613(1994)022<1091:SITMAF>2.3.CO;2.

Pratt, B.R., 1998a, Syneresis cracks: Subaqueous shrinkage in argillaceous sediments caused by earthquake-induced dewatering: Sedimentary Geology, v. 117, p. 1–10, https://doi.org/10.1016/S0037-0738(98)00023-2.

Pratt, B.R., 1998b, Molar-tooth structure in Proterozoic carbonate rocks: Origin from synsedimentary earthquakes, and implications for the nature and evolution of basins and marine sediment: Geological Society of America Bulletin, v. 110, p. 1028–1045, https://doi.org/10.1130/0016-7606(1998)110<1028:MTSIPC>2.3.CO;2.

Pratt, B.R., 2001, Oceanography, bathymetry and syndepositional tectonics of a Precambrian intracratonic basin: Integrating sediments, storms, earthquakes and tsunamis in the Belt Supergroup (Helena Formation, c. 1.45 Ga), western North America: Sedimentary Geology, v. 141–142, p. 371–394, https://doi.org/10.1016/S0037-0738(01)00083-5.

Pratt, B.R., 2002, Storms versus tsunamis: Dynamic interplay of sedimentary, diagenetic, and tectonic processes in the Cambrian of Montana: Geology, v. 30, p. 423–426, https://doi.org/10.1130/0091-7613(2002)030<0423:SVTDIO>2.0.CO;2.

Pratt, B.R., 2017, The Mesoproterozoic Belt Supergroup in Glacier and Waterton Lakes National Parks, northwestern Montana and southwestern Alberta: Sedimentary facies and syndepositional deformation, *in* Hsieh, J.C.C., ed., Geologic Field Trips of the Canadian Rockies: 2017 Meeting of the GSA Rocky Mountain Section: Geological Society of America Field Guide 48, p. 123–135, https://doi.org/10.1130/2017.0048(04).

Pratt, B.R., 2018, Discussion: "Depositional setting of the 2.1 Ga Francevillian macrobiota (Gabon): Rapid mud settling in a shallow basin swept by high-density sand flows" by Reynaud et al. (2018): Sedimentology, v. 65, p. 670–701, https://doi.org/10.1111/sed.12506.

Pratt, B.R., and Bordonaro, O.L., 2007, Tsunamis in a stormy sea: Middle Cambrian inner shelf limestones of western Argentina: Journal of Sedimentary Research, v. 77, p. 256–262, https://doi.org/10.2110/jsr.2007.032.

Pratt, B.R., and Haidl, F.M., 2008, Microbial patch reefs in Upper Ordovician Red River strata, Williston Basin, Saskatchewan: Signal of heating in a deteriorating epeiric sea, *in* Pratt, B.R., and Holmden, C., eds., The Dynamics of Epeiric Seas: Geological Association of Canada Special Paper 48, p. 303–340.

Pratt, B.R., and Holmden, C., 2008, Introduction, *in* Pratt, B.R., and Holmden, C., eds., The Dynamics of Epeiric Seas: Geological Association of Canada Special Paper 48, p. 1–5.

Price, R.A., 1964, The Precambrian Purcell System in the Rocky Mountains of southern Alberta and British Columbia: Bulletin of Canadian Petroleum Geology, v. 12, p. 399–426.

Price, R.A., and Sears, J.W., 2000, A preliminary palispastic map of the Mesoproterozoic Belt-Purcell Supergroup, Canada and USA: Implications for the tectonic setting and structural evolution of the Purcell anticlinorium and the Sullivan deposit, *in* Lydon, J.W., Höy, T., Slack, J.F., and Knapp, M.E., eds., The Geological Environment of the Sullivan Deposit, British Columbia: Geological Association of Canada, Mineral Deposits Division Special Publication 1, p. 61–81.

Ransom, P.W., and Lydon, J.W., 2000, Geology, sedimentology and evolution of the Sullivan sub-basin, *in* Lydon, J.W., Höy, T., Slack, J.F., and Knapp, M.E., eds., The Geological Environment of the Sullivan Deposit, British Columbia: Geological Association of Canada, Mineral Deposits Division Special Publication 1, p. 440–469.

Rezak, R., 1957, Stromatolites of the Belt Series in Glacier National Park and Vicinity: U.S. Geological Survey Professional Paper 294-D, p. 127–154, https://doi.org/10.3133/pp294D.

Rindsberg, A.K., 2005, Gas-escape structures and their paleoenvironmental significance at the Steven C. Minkin Paleozoic Footprint Site (Early Pennsylvanian, Alabama), *in* Buta, R.J., Rindsberg, A.K., and Kopaska-Merkel, D., eds., Pennsylvanian Footprints in the Black Warrior Basin of Alabama: Alabama Paleontological Society Monograph 1, p. 177–183.

Ross, C.P., 1959, Geology of Glacier National Park and the Flathead Region, Northwestern Montana: U.S. Geological Survey Professional Paper 296, 125 p., https://doi.org/10.3133/pp296.

Ross, G.M., and Villeneuve, M., 2003, Provenance of the Mesoproterozoic (1.45 Ga) Belt basin (western North America): Another piece in the pre-Rodinia paleogeographic puzzle: Geological Society of America Bulletin, v. 115, p. 1191–1217, https://doi.org/10.1130/B25209.1.

Ross, G.M., Parrish, R.R., and Winston, D., 1992, Provenance and U-Pb geochronology of the Mesoproterozoic Belt Supergroup (northwestern United States): Implications for age of deposition and pre-Panthalassa plate reconstructions: Earth and Planetary Science Letters, v. 113, p. 57–76, https://doi.org/10.1016/0012-821X(92)90211-D.

Rychliński, R., Jaglarz, P., Uchman, A., and Vainorius, J., 2014, Unusually well preserved casts of halite crystals: A case from the Upper Frasnian of northern Lithuania: Sedimentary Geology, v. 308, p. 44–52, https://doi.org/10.1016/j.sedgeo.2014.05.005.

Schieber, J., 2016, Mud re-deposition in epicontinental basins—Exploring likely processes: Marine and Petroleum Geology, v. 71, p. 119–133, https://doi.org/10.1016/j.marpetgeo.2015.12.014.

Sears, J.W., 2007a, Belt-Purcell Basin: Keystone of the Rocky Mountain fold-and-thrust belt, United States and Canada, *in* Sears, J.W., Harms, T.A., and Evenchick, C.A., eds., Whence the Mountains? Inquiries into the Evolution of Orogenic Systems: A Volume in Honor of Raymond A. Price: Geological Society of America Special Paper 433, p. 147–166, https://doi.org/10.1130/2007.2433(07).

Sears, J.W., 2007b, Rift destabilization of a Proterozoic epicontinental pediment: A model for the Belt-Purcell Basin, North America, *in* Link, P.K., and Lewis, R.S., eds., Proterozoic Geology of Western North America and Siberia: Society for Sedimentary Geology (SEPM) Special Publication 86, p. 55–64, https://doi.org/10.2110/pec.07.86.0055.

Shaw, A.B., 1964, Time in Stratigraphy: New York, McGraw-Hill, 365 p.

Slotznick, S.P., Winston, D., Webb, S.M., Kirschvink, J.L., and Fischer, W.W., 2016, Iron mineralogy and redox conditions during deposition of the mid-Proterozoic Appekunny Formation, Belt Supergroup, Glacier National Park, *in* MacLean, J.S., and Sears, J.W., eds., Belt Basin: Window to Mesoproterozoic Earth: Geological Society of America Special Paper 522, p. 221–242, https://doi.org/10.1130/2016.2522(09).

Smit, J., Laffra, C., Meuenaars, K., and Montanari, A., 2012, Probable late Messinian tsunamiites near Monte Dei Corvi, Italy, and the Nijar Basin, Spain: Expected architecture of offshore tsunami deposits: Natural Hazards, v. 63, p. 241–266, https://doi.org/10.1007/s11069-011-9947-9.

Spencer, R.J., and Demicco, R.V., 1993, Depositional environments of the Middle Cambrian Arctomys Formation, southern Canadian Rocky Mountains: Bulletin of Canadian Petroleum Geology, v. 41, p. 373–388.

Stockmal, G.S., and Fallas, K.M., compilers, 2015, Geology, Chinook South, Alberta–British Columbia: Geological Survey of Canada Open-File 7476, map scale 1:100,000, legend, and report, 48 p.

Talling, P.J., Masson, D.K., Sumner, E.J., and Malgesini, G., 2012, Subaqueous sediment density flows: Depositional processes and deposit types: Sedimentology, v. 59, p. 1937–2003, https://doi.org/10.1111/j.1365-3091.2012.01353.x.

Törő, B., and Pratt, B.R., 2015a, Eocene paleoseismic record of the Green River Formation, Fossil Basin, Wyoming, U.S.A.: Implications of synsedimentary deformation structures in lacustrine carbonate mudstones: Journal of Sedimentary Research, v. 85, p. 855–884, https://doi.org/10.2110/jsr.2015.56.

Törő, B., and Pratt, B.R., 2015b, Characteristics and implications of sedimentary deformation features in the Green River Formation (Eocene) in Utah and Colorado, *in* Vanden Berg, M.D., Ressetar, R., and Birgenheier, L.P., eds., Geology of Utah's Uinta Basin and Uinta Mountains: Utah Geological Association Publication 44, p. 371–422.

Törő, B., and Pratt, B.R., 2016, Sedimentary record of seismic events in the Eocene Green River Formation and its implications for regional tectonics on lake evolution (Bridger Basin, Wyoming): Sedimentary Geology, v. 344, p. 175–204, https://doi.org/10.1016/j.sedgeo.2016.02.003.

Toyofuku, T., Duros, P., Fontanier, C., et al., 2014, Unexpected biotic resilience on the Japanese seafloor caused by the 2011 Tohoku-Oki tsunami: Scientific Reports, v. 4, p. 7517, https://doi.org/10.1038/srep07517.

Trujillo, A.P., and Thurman, H.V., 2017, Essentials of Oceanography (12th ed.): Boston, Massachusetts, Pearson, 624 p.

Turner, R.J.W., Leitch, C.H.B., Höy, T., Ransom, P.W., Hagen, A., and Delaney, G.D., 2000, Sullivan graben system: District-scale setting of the Sullivan deposit, *in* Lydon, J.W., Höy, T., Slack, J.F., and Knapp, M.E., eds., The Geological Environment of the Sullivan Deposit, British Columbia: Geological Association of Canada, Mineral Deposits Division Special Publication 1, p. 370–407.

Tyrrell, S., Leleu, S., Souders, A.K., Haughton, P.D.W., and Daly, J.S., 2009, K-feldspar sand-grain provenance in the Triassic, west of Shetland: Distinguishing first-cycle and recycled sediment sources?: Geological Journal, v. 44, p. 692–710, https://doi.org/10.1002/gj.1185.

Uchman, A., Pika-Biolzi, M., and Hochuli, P.A., 2004, Oligocene trace fossils from temporary fluvial plain ponds: An example from the Freshwater Molasse of Switzerland: Eclogae Geologicae Helvetiae, v. 97, p. 133–148, https://doi.org/10.1007/s00015-004-1111-z.

Weiss, R., and Bahlburg, H., 2006, A note on the preservation of offshore tsunami deposits: Journal of Sedimentary Research, v. 76, p. 1267–1273, https://doi.org/10.2110/jsr.2006.110.

Whipple, J.W., compiler, 1992, Geologic Map of Glacier National Park, Montana: U.S. Geological Survey Miscellaneous Investigations Series Map I-1508-F, scale 1:100,000.

Whipple, J.W., and Johnson, S.N., 1988, Stratigraphy and Lithocorrelation of the Snowslip Formation (Middle Proterozoic Belt Supergroup), Glacier National Park, Montana: U.S. Geological Survey Bulletin 1833, 30 p.

Whipple, J.W., Connor, J.J., Raup, O.B., and McGimsey, R.G., 1984, Preliminary report on the stratigraphy of the Belt Supergroup, Glacier National Park and adjacent Whitefish Range, Montana, *in* McBane, J.D., and Garrison, P.B., eds., Northwest Montana and Adjacent Canada: Billings, Montana, Montana Geological Society, 1984 Field Conference and Symposium Guidebook, p. 33–50.

Wiberg, P.L., and Harris, C.K., 1994, Ripple geometry in wave-dominated environments: Journal of Geophysical Research, v. 99, p. 775–789, https://doi.org/10.1029/93JC02726.

Willis, B., 1902, Stratigraphy and structure, Lewis and Livingston ranges, Montana: Geological Society of America Bulletin, v. 13, p. 305–352, https://doi.org/10.1130/GSAB-13-305.

Wilson, R., and Schieber, J., 2017, Association between wave- and current-aided hyperpycnites and flooding surfaces in shelfal mudstones: An integrated sedimentologic, sequence stratigraphic, and geochemical approach: Journal of Sedimentary Research, v. 87, p. 1143–1155, https://doi.org/10.2110/jsr.2017.62.

Winston, D., 1986a, Sedimentology of the Ravalli Group, middle Belt carbonate and Missoula Group, Middle Proterozoic Belt Supergroup, Montana, Idaho and Washington, *in* Roberts, S.M., ed., Belt Supergroup: A Guide to Proterozoic Rocks of Western Montana and Adjacent Areas: Montana Bureau of Mines and Geology Special Publication 94, p. 85–124.

Winston, D., 1986b, Middle Proterozoic tectonics of the Belt Basin, western Montana and northern Idaho, *in* Roberts, S.M., ed., Belt Supergroup: A Guide to Proterozoic Rocks of Western Montana and Adjacent Areas: Montana Bureau of Mines and Geology Special Publication 94, p. 245–257.

Winston, D., 1986c, Sedimentation and tectonics of the Middle Proterozoic Belt Basin and their influence on Phanerozoic compression and extension in western Montana and northern Idaho, *in* Peterson, J.A., ed., Paleotectonics and Sedimentation in the Rocky Mountain Region, United States: American Association of Petroleum Geologists Memoir 41, p. 87–118.

Winston, D., 1989a, Introduction to the Belt, *in* Winston, D., Horodyski, R.J., and Whipple, J.W., eds., Middle Proterozoic Belt Supergroup, Western Montana: Washington, D.C., American Geophysical Union, 28th International Geological Congress Field Trip Guidebook T334, p. 1–6.

Winston, D., 1989b, A sedimentologic and tectonic interpretation of the Belt, *in* Winston, D., Horodyski, R.J., and Whipple, J.W., eds. Middle Proterozoic Belt Supergroup, Western Montana: Washington, D.C., American Geophysical Union, 28th International Geological Congress Field Trip Guidebook T334, p. 46–69.

Winston, D., 1990, Evidence for intracratonic, fluvial and lacustrine settings of middle to late Proterozoic basins of western U.S.A., *in* Gower, C.F., Rivers, T., and Ryan, B., eds., Mid-Proterozoic Laurentia–Baltica: Geological Association of Canada Special Paper 38, p. 535–564.

Winston, D., 2007, Revised stratigraphy and depositional history of the Helena and Wallace formations, mid-Proterozoic Piegan Group, Belt Supergroup, Montana and Idaho, U.S.A., *in* Link, P.K., and Lewis, R.S., eds.,

Proterozoic Geology of Western North America and Siberia: Society for Sedimentary Geology (SEPM) Special Publication 86, p. 65–100, https://doi.org/10.2110/pec.07.86.0065.

Winston, D., 2016, Sheetflood sedimentology of the Mesoproterozoic Revett Formation, Belt Supergroup, northwestern Montana, USA, *in* MacLean, J.S., and Sears, J.W., eds., Belt Basin: Window to Mesoproterozoic Earth: Geological Society of America Special Paper 522, p. 1–56, https://doi.org/10.1130/2016.2522(01).

Winston, D., and Link, P.K., 1993, Middle Proterozoic rocks of Montana, Idaho and eastern Washington: The Belt Supergroup, *in* Link, P.K., ed., Middle and Late Proterozoic Stratified Rocks of the Western U.S. Cordillera, Colorado Plateau, and Basin and Range Province, *in* Reed, J.C., Bickford, M.E., Houston, R.S., Link, P.K., Rankin, D.W., Sims, P.K., and Van Schmus, W.R., eds., Precambrian: Conterminous U.S.: Boulder, Colorado, Geological Society of America, The Geology of North America, v. C-2, p. 487–517.

Winston, D., and Sears, J.W., 2013, Stratigraphy of the Proterozoic Belt Supergroup and structure of the Belt Basin: Glacier National Park and Blackfoot River Canyon, Montana, Part I: Glacier National Park, *in* Belt Symposium V: Northwest Geology, v. 42, p. 237–256.

Winston, D., and Smith, A.V., 2016, Crinkle cracks in the Proterozoic Piegan Group, Belt Supergroup, Montana and Idaho: A descriptive style of sand-filled cracks hypothetically formed by subaqueous solitary-like waves, *in* MacLean, J.S., and Sears, J.W., eds., Belt Basin: Window to Mesoproterozoic Earth: Geological Society of America Special Paper 522, p. 57–69, https://doi.org/10.1130/2016.2522(02).

Winston, D., McGee, D., and Quattlebau, D., 1986, Stratigraphy and sedimentology of the Bonner Formation, Middle Proterozoic Belt Supergroup, western Montana, *in* Roberts, S.M., ed., Belt Supergroup: A Guide to Proterozoic Rocks of Western Montana and Adjacent Areas: Montana Bureau of Mines and Geology Special Publication 94, p. 182–195.

Zavala, C., Ponce, J.J., Arcuri, M., Drittanti, D., Freije, H., and Asensio, M., 2006, Ancient lacustrine hyperpycnites: A depositional model from a case study in the Rayoso Formation (Cretaceous) of west-central Argentina: Journal of Sedimentary Research, v. 76, p. 41–59, https://doi.org/10.2110/jsr.2006.12.

Zavala, C., Arcuri, M., Di Meglio, M., Gamero Diaz, H., and Contreras, C., 2011, A genetic facies tract for the analysis of sustained hyperpycnal flow deposits, *in* Slatt, R.M., and Zavala, C, eds., Sediment Transfer from Shelf to Deep Water—Revisiting the Delivery System: American Association of Petroleum Geologists (AAPG) Studies in Geology 61, p. 31–51.

Science Editor: Rob Strachan
Associate Editor: Robert Rainbird

Manuscript Received 17 April 2018
Revised Manuscript Received 14 October 2018
Manuscript Accepted 5 December 2018

Printed in the USA